




A new phytosaur species (Archosauriformes) from the Upper Triassic of Jameson Land, central East Greenland

Víctor López-Rojas, Lars B. Clemmensen, Jesper Milàn, Oliver Wings, Nicole Klein & Octávio Mateus

To cite this article: Víctor López-Rojas, Lars B. Clemmensen, Jesper Milàn, Oliver Wings, Nicole Klein & Octávio Mateus (2023): A new phytosaur species (Archosauriformes) from the Upper Triassic of Jameson Land, central East Greenland, *Journal of Vertebrate Paleontology*, DOI: [10.1080/02724634.2023.2181086](https://doi.org/10.1080/02724634.2023.2181086)

To link to this article: <https://doi.org/10.1080/02724634.2023.2181086>

 View supplementary material 

 Published online: 24 Mar 2023.

 Submit your article to this journal 

 View related articles 

 View Crossmark data 

A NEW PHYTOSAUR SPECIES (ARCHOSAURIFORMES) FROM THE UPPER TRIASSIC OF JAMESON LAND, CENTRAL EAST GREENLAND

VÍCTOR LÓPEZ-ROJAS, ^{1*} LARS B. CLEMMENSEN, ² JESPER MILÀN, ³ OLIVER WINGS, ⁴ NICOLE KLEIN, ^{5,6}
and OCTÁVIO MATEUS ¹

¹ GeoBioTec, FCT-UNL Faculdade de Ciências e Tecnologia, Universidade Nova de Lisboa, 2829-516 Monte da Caparica, Portugal; Museu da Lourinhã, Portugal. v.rojas@campus.fct.unl.pt*; omateus@fct.unl.pt;

² Department of Geosciences and Natural Resource Management, University of Copenhagen, Øster Voldgade 10, DK-1350 Copenhagen K, Denmark. larsc@ign.ku.dk;

³ Geomuseum Faxe, Rådhusvej 2, DK-4640 Faxe, Denmark. jesperm@oesm.dk;

⁴ Natural History Museum Bamberg, Fleischstr. 2, 96047 Bamberg, Germany. wings@snsb.de;

⁵ Division of Paleontology, Institute of Geoscience, University of Bonn, Nußallee 8, 53115 Bonn, Germany. nklein@posteo.de;

⁶ Paleontological Institute and Museum, University of Zurich, Zurich, Switzerland

ABSTRACT—Herein we describe phytosaurs from thin fluvial overbank sandstones of the Upper Triassic Malmros Klint Formation of the Fleming Fjord Group (central East Greenland). The new sample includes more than 150 disarticulated bones and teeth from small to large specimens belonging to at least four individuals. The fossils mostly consist of teeth and postcranial elements and permit the recognition of a new species of *Myrstriosuchus*, *M. alleroq*, diagnosed by an L-shaped quadratojugal whose anterior suture trends anterodorsally and a tripartite degree of heterodonty. Humeral diaphyseal histology of one specimen reveals a fairly compact cortex that surrounds a cancellous medullary region followed by a remodeling zone containing scattered secondary osteons. Primary bone tissue is parallel-fibred with a moderate to low vascular density. The cortex is cyclically interrupted by distinct growth marks indicating a seasonal environment. A change in growth rate from moderate to low is documented within the outer cortex, indicating that at least this individual was close to somatic maturity. *Myrstriosuchus* has formerly been known as an exclusively European taxon. The new findings support the European faunal influence in East Greenland during the Late Triassic inferred from other taxa such as temnospondyls and archosaurs. The mid-late Norian age of European *Myrstriosuchus* suggests an additional age constraint for the vertebrate-bearing portion of the Malmros Klint Formation.

<http://zoobank.org/urn:lsid:zoobank.org:pub:4F91184A-4207-45ED-8214-D503161EA248>

SUPPLEMENTAL DATA—Supplemental materials are available for this article for free at www.tandfonline.com/UJVP.

Citation for this article: López-Rojas, V., L. B. Clemmensen, J. Milàn, O. Wings, N. Klein, and O. Mateus. (2023) A new phytosaur species (Archosauriformes) from the Upper Triassic of Jameson Land, central East Greenland. *Journal of Vertebrate Paleontology*. <https://doi.org/10.1080/02724634.2023.2181086>

Submitted: February 9, 2022

Revisions received: December 19, 2022

Accepted: January 9, 2023

INTRODUCTION

In the Late Triassic, freshwater environments were mainly dominated by archosauriforms, in particular the crocodile-like phytosaurs. Phytosaurs were originally described by Jäger (1828) as herbivorous reptiles, but von Meyer and Plieninger (1844) more accurately interpreted them as semi-aquatic carnivorous animals with a similar lifestyle to extant crocodylians. Phytosaurs are characterized by two main traits in their skulls: (1) a strongly dorsoventrally compressed skull with mainly dorsally placed antorbital fenestrae and orbits; and (2) external nostrils displaced dorsally and posteriorly, reaching the anterior edge of the orbits (Ezcurra, 2016).

Phytosaurs have a global distribution with a very rich fossil record in Laurasia. Occurrences are known from central Europe (Dzik, 2001; Kimmig and Arp, 2010; Brusatte et al., 2013; Butler et al., 2019), southern Europe (Gozzi & Renesto, 2003; Mateus et al., 2014a), North America (Stocker, 2010), and Asia (Buffetaut & Ingavat, 1982; Buffetaut et al., 1988; Li et al., 2012). Fossil remains have also been discovered in Gondwana with occurrences in North Africa (Lagnaoui et al., 2016), South Africa (Burmeister et al., 2006; Barrett et al., 2020), South America (Kischlat and Lucas, 2003), and India (Datta et al., 2019, 2021). Stratigraphically, they range from in the upper Middle Triassic (Ladinian, *Diandongosuchus fuyuanensis* Stocker et al., 2017) to the uppermost Triassic (upper Norian?–Rhaetian, *Redondasaurus gregorii* Hunt and Lucas, 1993). Conceivably, older taxa (*Mesorhinosuchus fraasi*, Jaekel, 1910, Lower Triassic of Germany) as well as younger taxa (Early Jurassic; Maisch & Kapitzke, 2010) could belong to Phytosauria. However, this is unclear because the holotype of *M. fraasi* was destroyed during World War II, so its provenance

* Corresponding author.

Color versions of one or more of the figures in the article can be found online at www.tandfonline.com/ujvp.

and age has been questioned repeatedly (Gregory, 1969; Hunt & Lucas, 1991), and the Early Jurassic phytosaur fossils need further studies (Stocker and Butler, 2013).

The phylogenetic relationships among phytosaurs, crocodylians, and other archosaurs have been the subject of much debate and controversy ever since their discovery. They were first included within Thecodontia (Owen, 1859), a now obsolete clade which placed emphasis on their relationship to modern crocodylians (Colbert, 1947; Buffetaut & Ingavat, 1982). McGregor (1906) soon differentiated the phytosaurs from the crocodylian lineage and suggested that similar morphological features in both groups were homoplastic. However, their higher nomenclature is still not well resolved, and an updated scheme was suggested by Kischlat (2022). Modern phylogenies support no close relationship between phytosaurs and crocodylians (Serenó, 1991; Stocker & Butler, 2013), and more recent studies focus on the relationships among phytosaurs and other archosaurs. Some describe them as the sister-taxa of Archosauria (Nesbitt, 2011) while others place them within Archosauria, as the sister-taxon of Pseudosuchia (Ezcurra, 2016). Unraveling the phylogenetic affinities of phytosaurs depends on both new discoveries and analyses.

Here we describe an unusually rich phytosaur bone assemblage from the Upper Triassic of central East Greenland, representing a growth series of several individuals. The earliest description of possible Greenland phytosaur remains is from Jenkins et al. (1994). However, those remains are fragmentary (Sulej et al., 2014) and in need of revision. Here, we provide the first detailed description of unequivocally Greenlandic phytosaur material, with a preliminary phylogenetic analysis and a discussion of our findings within paleoclimatic and paleogeographic contexts.

Geological Setting

Upper Triassic sediments are well exposed in the Jameson Land Basin, which is located in central East Greenland at about 71°N near the areas of present-day Jameson Land and Scoresby Land (Fig. 1A; Clemmensen et al., 2016, 2020). During the Late Triassic, the Basin was located at the northern rim of the Pangaea supercontinent at approximately 43°N (Kent et al., 2014; Kent and Clemmensen, 2021). The Basin was placed in a transition zone between the relatively dry interior of the supercontinent Pangaea and the more humid peripheral part of this continent (Clemmensen et al., 1998; Sellwood and Valdes, 2006), or well within the humid temperate belt (Kent et al., 2014; Mau et al., 2022). The Jameson Land Basin was situated at the southern end of the East Greenland rift system, which formed part of a larger rift complex separating Greenland from Norway prior to the opening of the Atlantic (Nøttvedt et al., 2008; Guarnieri et al., 2017). In the Late Triassic (Norian), the Boreal Sea was situated far to the north of the basin (Andrews and Decou, 2019).

The Jameson Land Basin was bounded by the N–S stretching Liverpool Land to the east and the Stauning Alper to the west. To the north and south, the basin was demarcated by a fracture zone in the Kong Oscars Fjord and the Scoresby Sund, respectively (Fig. 1; Guarnieri et al., 2017; Clemmensen et al., 2020). Since the Late Triassic, the Basin has been rotated 45° clockwise and translated 30° northward relative to present-day meridians (Kent & Tauxe, 2005).

Upper Triassic sediments in the Jameson Land Basin comprise the complete Fleming Fjord Group (Clemmensen et al., 2020; Kent & Clemmensen, 2021); parts of the underlying Gipsdalen Group may also be of Late Triassic (Carnian) age (Andrews et al., 2014; Clemmensen et al., 2020). The Fleming Group consists of three formations, the Edderfugledal Formation at the base, the Malmros Klint Formation in the middle, and the Ørsted Dal Formation on top (Fig. 1B, C). The total thickness of the Fleming Fjord Group is about 350 m, with some variation

across the basin (Clemmensen et al., 2020). The Edderfugledal and Malmros Klint formations formed in shallow lacustrine/playa lake environments; a large portion of the Ørsted Dal Formation (the Carlsberg Fjord and Tait Bjerg members) also records lake deposition, whereas part of this formation (the Bjergkronerne Member) records fluvial sedimentation (Clemmensen et al., 1998, 2016, 2020).

New paleomagnetic work (Kent and Clemmensen, 2021) indicates that the Fleming Fjord Group was deposited between 220 and 209 Ma (Middle to Late Norian). The phytosaur fossils described here are from the thin interval in the middle part of the Malmros Klint Formation (Fig. 1C) and dated to 214.8 Ma (mid-Norian).

Phytosaur remains were found in a 1 m thick stratigraphic interval in the middle part of the Malmros Klint Formation 65 m above the base of the formation. Bone remains were primarily found in three 5–20 cm thick, fine-grained sandstone beds that can be traced up to 200 m laterally. The bone-bearing sandstones are closely associated with red, massive to weakly laminated lacustrine mudstones with frequent desiccation features. Within the bonebed site, the lowermost layer was particularly rich in phytosaur remains. During the second field season, the quarry was expanded to cover a total area of 15 m². The total thickness of the exposed sediment was approximately 1 m from the quarry site and within the same stratigraphic level a poorly exposed fluvial channel sandstone is also present. The bone-bearing thin sandstone layers can therefore be interpreted as fluvial channel margin/overbank deposits.

Vertebrate Assemblage

The Fleming Fjord Group of East Greenland (Clemmensen et al., 2020) comprises a diverse faunal assemblage containing chondrichthyans and actinopterygian fishes, lungfish such as *Ceratodus tenuensis* (Agnolin et al., 2018), theropod and sauropodomorph dinosaurs, temnospondyls, turtles, aetosaurs, phytosaurs, and pterosaurs (Jenkins et al., 1994, 2001; Sulej et al., 2014; Clemmensen et al., 2016; Marzola et al., 2017a, 2018; Agnolin et al., 2018; Niedźwiedzki and Sulej, 2020; Beccari et al., 2021; Milàn et al., 2021). Furthermore, the fauna includes both teeth and skeletal elements of early mammaliaforms (Jenkins et al., 1994; Shapiro & Jenkins, 2001; Sulej et al., 2020; Beccari et al., 2021). Tracks and trackways provide evidence for abundant small to medium-sized theropod dinosaurs, sauropods, and sauropodomorphs spanning a large range of body sizes and other archosaurs (Clemmensen et al., 2016; Sulej et al., 2014; Klein et al., 2016; Lallensack et al., 2017). The phytosaur remains described here were briefly mentioned by Clemmensen et al. (2016), Marzola et al. (2017a), and Marzola (2019).

MATERIAL AND METHODS

The current study is based on 150 bones and teeth collected during two expeditions to Lepidopteris Elv at the eastern margin of the Jameson Land Basin in 2012 and 2016 (Table S1; Mateus et al., 2014b; Marzola et al., 2017a) deposited at the NHMD. Most of the material was mechanically prepared with pneumatic air scribes, HW10 and HW322 (Marzola, 2019), with the rest of the material prepared by ML technicians. Broken parts were glued with 50% Paraloid B72 in acetone. Photographs were taken using a Canon EOS 350 Digital DS126071, and a DinoLite AM411T for the serration counting observed in the teeth. Interpretative designs were done using the Wacom Intuos Pro digital drawing tablet and pen.

Measurements of the fossil material were taken with ImageJ software. For measurements of the fossil teeth, they were described following the terminology from Hendrickx et al. (2015), while identified and measured following Hungerbühler

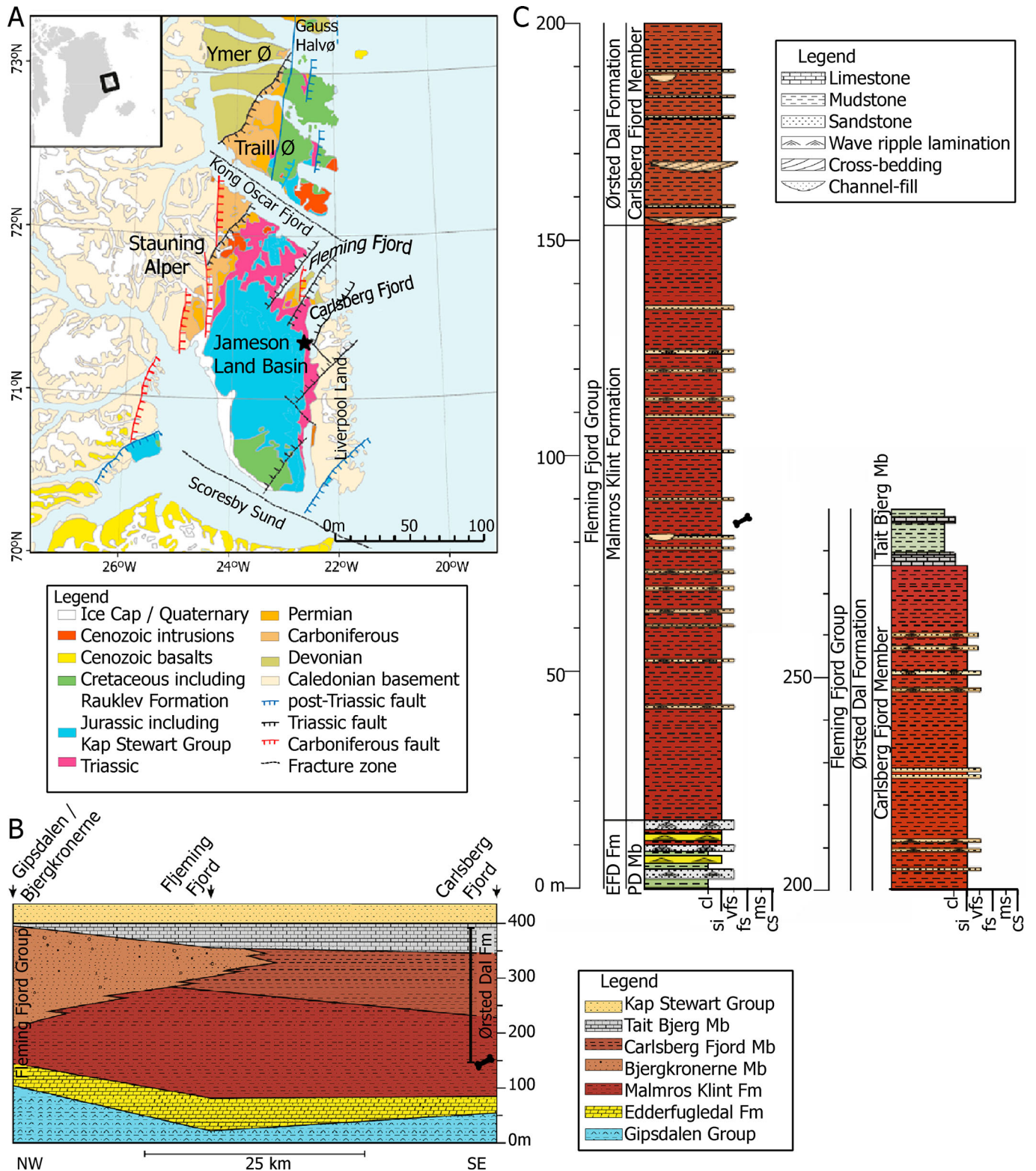


FIGURE 1. **A**, geological map of East Greenland with the Jameson Land Basin (from Clemmensen et al., 2020); **B**, Fleming Fjord Group cross section of the lithostratigraphic units (from Clemmensen et al., 2020); **C**, section of the lithostratigraphic units in Fleming Fjord Group at *Lepidopteris* Elv. The Fleming Fjord group (**B**) is marked with a star in **A**. The phytosaur site is indicated with a bone in **B** and **C**, situated at 82 m in the middle part of the Malmros Klint Formation (from Clemmensen et al., 2020).

(2000; Fig. 4). Even though Hendrickx et al. (2015) focused on theropod teeth, the anatomical nomenclature is more updated than the one from Hungerbühler (2000). All the measurements are in millimeters.

The midshaft of the right humerus of NHMD-916843 was removed and replaced by plaster (Fig. 10). The cross section was processed into a petrographic thin section using standard methods (Klein and Sander, 2007) with histological terminology following Francillon-Vieillot et al. (1990). The thin section was studied under a Leica DM2500LP polarizing microscope. Digital photomicrographs were taken with a Leica DFC420 mounted color camera and edited using the 2007 Leica Image Access EasyLab 7 software. The ratio between the medullary and cortical region along with bone density were measured with a pixel-counting computer program (©Peter Göddertz, IGPB). High-resolution images of the histological slides have been uploaded to Morphobank, with project number P44641.

For the phylogenetic analysis, TnT version 1.5 (Goloboff and Catalano, 2016) was used. We used the Jones and Butler (2018) dataset composed of 43 operational taxonomic units (OTUs) plus the Greenland phytosaur and the 94 characters related to the cranial region, plus one additional character (number 95) about the degree of heterodonty, adapted from Hungerbühler (2002; character 5: 0–homodont, 1–bipartite upper dentition, 2–tripartite upper dentition). The heuristic analysis of maximum parsimony was done with 1000 random replications and saving 10 trees per replication.

The “degree of heterodonty” was added into the matrix of Jones and Butler (2018) because of the large number of teeth discovered. Only 11 species (*Mystriosuchus planirostris* von Meyer, 1863; *Nicrosaurus kapffi* Fraas, 1866; *Machaeropsopus buceros* Cope, 1881; *Euparkeria capensis* Broom, 1913; *Machaeropsopus pristinus* Mehl, 1928a; *Ebrachosuchus neukami* Kuhn, 1936; *Machaeropsopus mccauleyi* Ballew, 1989; *Redondasaurus bermani* Hunt and Lucas, 1993; *Redondasaurus gregorii* Hunt and Lucas, 1993; *Mystriosuchus westphali* Hungerbühler and Hunt, 2000; and *Nicrosaurus meyeri* Hungerbühler and Hunt, 2000) appeared in both Hungerbühler (2002) and the analysis of Jones and Butler (2018). Six species were added (*Rutiodon carolinensis* Emmons, 1856; *Parasuchus hislopi* Lydekker, 1885; *Angistorhinus grandis* Mehl, 1913; *Leptosuchus crosbiensis* Case, 1922; *Paleorhinus parvus* Mehl, 1928b; and *Angistorhinus talaiti* Dutuit, 1977) from Hungerbühler (2000) to complete the matrix.

Nomenclature Acts—This article follows the requirements of the International Code of Zoological Nomenclature (ICZN) and, therefore, the new name is available under this Code. The work and the nomenclature acts contained here have been registered in ZooBank, the online registration system of the ICZN. The ZooBank LSIDs (Life Science Identifiers) for this publication is 4F91184A-4207-45ED-8214-D503161EA248.

Institutional Abbreviations

MB, Museum für Naturkunde, Berlin, Germany; **ML**, Museu da Lourinhã, Lourinhã, Lisbon, Portugal; **NHMD**, Natural History Museum of Denmark, University of Copenhagen, Copenhagen, Denmark; **NHMW**, Naturhistorisches Museum Wien, Vienna, Austria; **NMMNHS**, New Mexico Museum of Natural History and Science, Albuquerque, U.S.A.; **PEFO**, Petrified Forest National Park, Arizona, U.S.A.; **SMNS**, Staatliches Museum für Naturkunde Stuttgart, Stuttgart, Germany; **TTU**, Museum of Texas Tech University, Paleontology Division, Lubbock, Texas, U.S.A.; **UMMP**, University of Michigan Museum of Paleontology, Ann Arbor, Michigan, U.S.A.

SYSTEMATIC PALEONTOLOGY

PHYTOSAURIA Jäger, 1828

PARASUCHIDAE Lydekker, 1885

MYSTRIOSUCHINAE von Huene, 1915

LEPTOSUCHOMORPHA Stocker, 2010

MYSTRIOSUCHINI von Huene, 1915

MYSTRIOSUCHUS Fraas, 1896

Type Species—*Mystriosuchus planirostris* (von Meyer, 1863).

Diagnosis—Interpremaxillary fossa present, narrow slit-like; interorbital nasal area dorsally curved in cross section (see character list, node 69).

MYSTRIOSUCHUS ALLEROQ, sp. nov.

Diagnosis—Autapomorphies of taxon: quadratojugal L-shaped, anterior suture trends anterodorsally (character 68); degree of heterodonty: tripartite upper dentition (character 95).

Differential Diagnosis—It differs from other species of *Mystriosuchus* by (1) the diastema-like structure in the posterior region of the terminal rosette of the premaxilla (Fig. 2A); (2) absence of a “narial crest,” as it displays a less abrupt and more gradual transition between the maxilla and nasal of the dorsal region of the rostrum (Fig. 2A) in contrast to *M. planirostris* and more similar to *M. westphali* or *M. steinbergeri*; (3) a “secondary coronoid” projection of the surangular anteriorly distal from the glenoid and more dorsally projected (Figs. 3B, D, 11E, G); (4) in contrast with the absence of the premaxillary crest, more similar to *M. planirostris*.

Etymology—*alleroq* means jawbone in Greenlandic.

Holotype—NHMD-916731 (nearly complete left mandible; Fig. 3), currently (2022) on display at GeoCenter Møns Klint, Denmark.

Paratype—NHMD-916728 (partial left quadratojugal; Fig. 2E).

Referred Material—Teeth, cranial, and postcranial bones from at least four individuals of different ontogenetic ages, all from the same site. See the complete list including collection numbers in Table S1.

Horizon, Locality, and Age—In Mateus Quarry (N71°15.584' W22°31.798', 171 m asl ±3 m), at Lepidopteris Elv locality (also written as Lepidopteriselv), Jameson Land Basin, central East Greenland. In the middle of Malmros Klint Formation, Fleming Fjord Group (82 m, Clemmensen et al., 2020). Mid Norian (214.8 Ma), Late Triassic.

DESCRIPTION

Skull and Mandible

A total of 13 bones referable to the skull and mandible (Figs. 2, 3, S1, Table S2) have been collected.

Cranium—From the rostrum, a partial right rostrum NHMD-916722 (Fig. 2A), represented by the right premaxilla and partial right maxilla, and an incomplete left premaxilla (NHMD-916721; Fig. S1A) were found. Both are long slender bones, with alveoli preserved that can be seen in ventral and partially in lateral views (NHMD-916721 with eight alveoli, and NHMD-916722 with 36 alveoli), which varies from subcircular (anterior positions) to elliptical (posterior ones). The dorsal rostral region of NHMD-916722 projects slightly posterodorsally by the level of the 21st and 23rd alveoli (counting starting from the first premaxillary alveolus). The terminal rosette of both premaxillae is constricted between the fourth and fifth teeth, with the anteriormost part ventrally turned, creating a diastema-like structure that differentiates it from the rest of the rostrum. Medially, the interpremaxillary fossa is preserved in NHMD-916722 as a smoother and

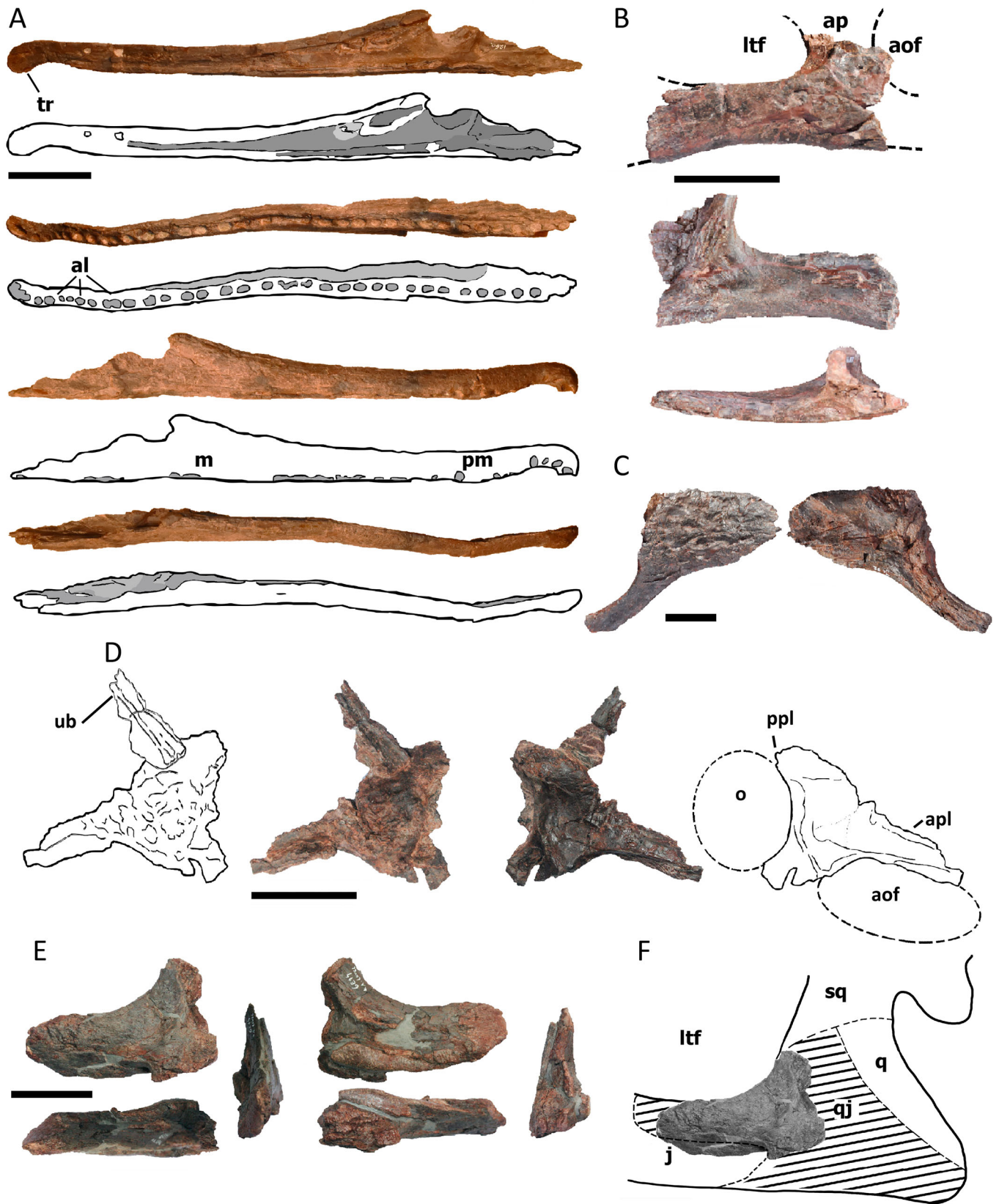


FIGURE 2. Cranial material of *Mystriosuchus alleroq*, sp. nov. **A**, partial right rostrum NHMD-916722 and interpretative drawings (labial, ventral, lingual, and dorsal views); **B**, right jugal NHMD-916733 (labial, lingual, and ventral views); **C**, left postorbital NHMD-916725 (dorsal and ventral views); **D**, left lacrimal NHMD-916729 and interpretative drawings (dorsal and ventral views); **E**, left quadratojugal NHMD-916728 (lateral, dorsal, anterior, medial, ventral, and posterior views); **F**, interpretative drawing of the quadratojugal position and morphology in the skull. Gray areas represent fossae or deeper areas. Cross-hatched area is the interpretative display of the complete bone. Dashed lines represent the interpretative limits of bones or fenestrae. **Abbreviations:** al, alveolus; aof, antorbital fenestra; ap, ascending process of the jugal; apl, anterior process of the lacrimal; j, jugal; ltf, lateral temporal fenestra; m, maxilla; o, orbit; pm, premaxilla; ppl, posterior process of the lacrimal; q, quadrate; qj, quadratojugal; sq, squamosal; tr, terminal rosette; ub, unidentified bone. Scale bars equal 4 cm.

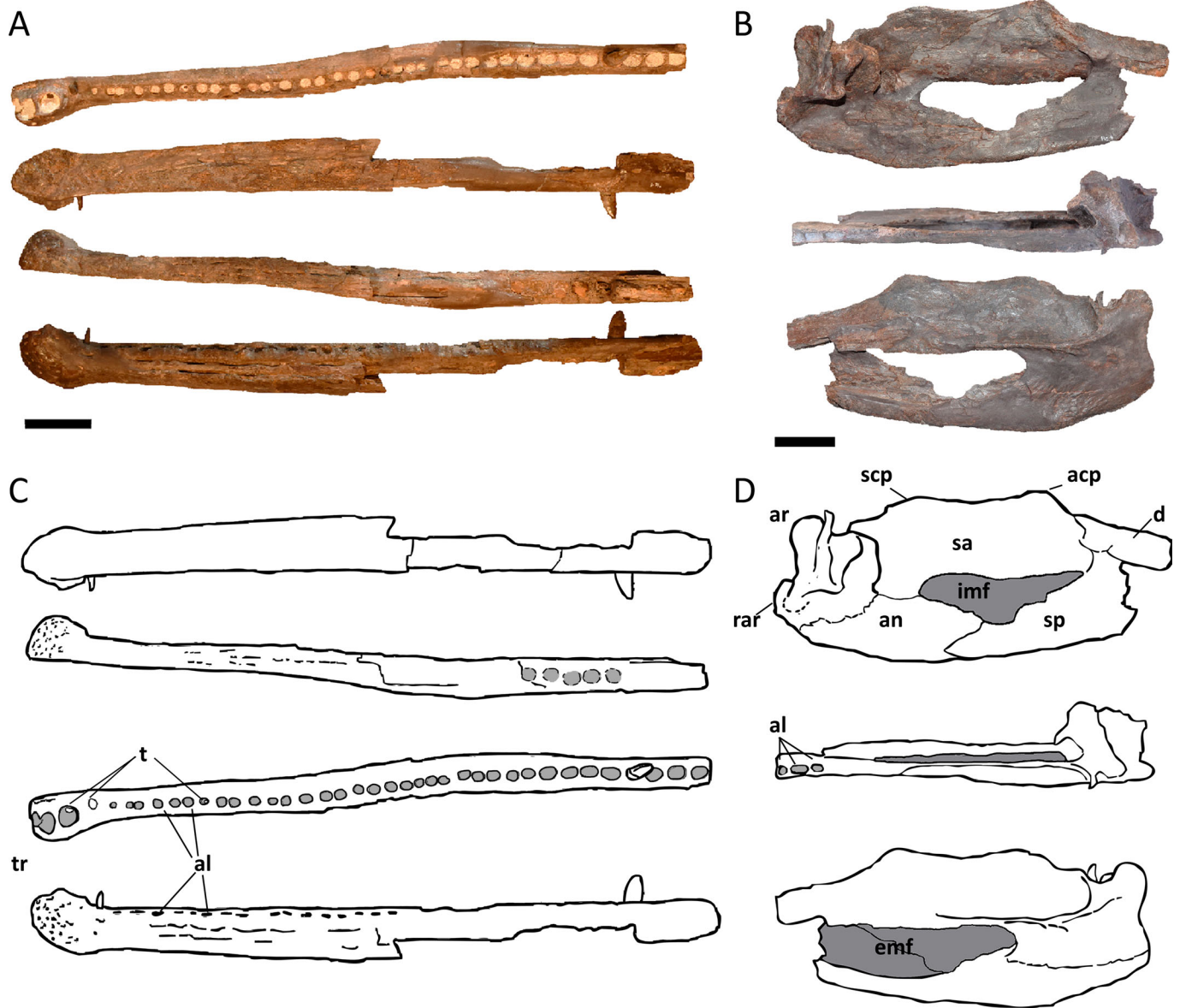


FIGURE 3. Holotype mandible of *Myrstriosuchus alleroq*, sp. nov., NHMD-916731. **A**, left dentary (dorsal, lingual, ventral, and labial views); **B**, left posterior body of the mandible (lingual, dorsal, and labial views); **C**, **D**, Interpretative drawings of **A**, **B**, respectively. Light gray areas represent the alveoli fossae. Dark gray areas represent the fenestrae. **Abbreviations:** **acp**, anterior coronoid process of the surangular; **al**, alveolus; **an**, angular; **ar**, articular; **d**, dentary; **emf**, external mandibular fenestra; **imf**, internal mandibular fenestra; **rar**, retroarticular process; **sa**, surangular; **scp**, secondary coronoid process of the surangular; **sp**, splenial; **t**, tooth; **tr**, terminal rosette. Scale bars equal 4 cm.

concave region that extends from the fifth tooth until the posterior and dorsal borders of the maxilla. The preserved portion of the maxilla of NHMD-916722 is thicker posteriorly than anteriorly and ventrally than dorsally, with the contacts between premaxilla-maxilla difficult to distinguish. Posteriorly, the maxilla has a triangular shape that contacts the jugal. The labial surface of the maxilla is slightly concave, in contrast with the smooth and straight labial surface of the premaxilla.

Only the main anterior body is preserved in the two jugals (NHMD-916723 and NHMD-916724; right and left respectively; Figs. 2B, S1B). They are rectangular with a weakly concave ventral margin (less markedly than in NHMD-916723, due to breakage). A portion of the anterior ascending process is also preserved, which dorsally contacts the ventral border of the lacrimal and anteriorly contacts the posterior maxilla. However, it is

broken and the contact with the orbit is not preserved. The suture with the maxilla is visible in NHMD-916724 as a scar on its anteroventral region in labial view. Its posterior and dorsal edges make a concave curve, being part of the anteroventral region of the lateral temporal fenestra. In NHMD-916724, the anterior edge has a smooth anterior concave surface similar to the posterodorsal edges.

The left postorbital NHMD-916725 (Fig. 2C) preserves the descending process that contacts with the jugal dorsally. The descending process is slender and expands anteroventrally. It has an anterior smooth and concave surface that would form part of the posterior border of the orbit. The posterior surface of the descending process is straighter and formed part of the anterior border of the lateral temporal fenestra. The dorsal surface is strongly ornamented with pits whereas the ventral surface is smooth.

NHMD-916729 (Fig. 2D) represents a partial left lacrimal, with most of its central part preserved. It is subtriangular with three processes: an anterior process, which is the longest and thinnest, with a concave lateral surface in its ventral region; a posterior process, which is thicker in its medial region with a concave ventrolateral depression; and a short middle process with a slightly concave region along both the anterior and posterior edges. The continuity between the lateral surfaces of anterior and posterior processes indicates that they form the margins of two different fenestrae: the posterior region of the antorbital fenestra and the anterior region of the orbit. The central dorsal area of the lacrimal has a pitted ornamentation. Attached to the lacrimal, there is a long thin rectangular element of an unidentified bone.

NHMD-916728 (Fig. 2E, F) represents the anterior region of a left quadratojugal. It is a mediolaterally compressed bone, anterodorsally bowed, that becomes thicker posteriorly. It has two short broken processes along its ventral region, one anterior and another posterior. The smooth slight curvature along its anterodorsal margin is the posteroventral border of the lateral temporal fenestra, whereas the dorsal margin would contact the ventral squamosal region, following the border of the lateral temporal fenestra. The anteromedial edge has a rough surface, interpreted as an articular facet, which would contact with the posterodorsal ramus of the jugal. In the lateral anterior region of the quadratojugal, there is a ventrally facing concavity that would encase the posteriormost jugal ramus. The posterior region is broken, but it displays a concavity where the quadrate would fit.

The partial left quadrate NHMD-916726 (Fig. S1C) preserves most of the medial portion. The ventral surface is smoother anteriorly than posteriorly. Posteriorly, the ventral surface has an articular facet with the articular. The lateral condyle is more expanded laterally than the medial condyle is medially, with a triangular shape and a more rounded shape, respectively. The medial surface of the quadrate has a bulge dividing the dorsal region, that would contact the pterygoid, from the ventral region, which faced the oral cavity.

The broken bone NHMD-916727 (Fig. S1D) is interpreted as a partial left posterior ectopterygoid. Its posterior region is wider than its anterior region and the medial edge is slightly bowed. Ventrally, the surface is rugose and flat, the rugosity potentially being musculature scars as there are no patterns as in ornamented bones. Dorsally, a convex lateral edge turns into a flatter surface laterally, likely representing the left choana. The medial dorsal surface shows a slight depression, forming the contact with the pterygoid, that posteromedially expands, giving the posterior end a triangular shape.

Lower Jaw—The holotype (NHMD-916731), a nearly complete left mandible, is broken at the posterior dentary, dividing it into an almost complete dentary with a total of 42 alveoli (Fig. 3A, C; with four teeth still attached, see Teeth section), and the posterior body (Fig. 3B, D). The holotype is missing most of splenial, and the ventral and labial regions after the 21st tooth height. The dentary is long, straight, and robust, displaying a faintly sigmoidal shape in dorsal view, with the lingual surface smoother than the labial. The dentary is straight until the 22nd alveoli tooth, where it becomes thicker distal-lingually. It has a terminal rosette with four teeth, and a constriction between the fourth and fifth teeth (as in the premaxillae NHMD-916721 and NHMD-916722), which displays a pitting pattern on its surface. There are some conjoined alveoli, such as the 6th–7th, and 15th–16th, as seen in *Machaeropsopus* (Heckert et al., 2013). The alveoli are bigger and closer in between in posterior positions, after the 27th alveolus, where it becomes difficult to tell if they are conjoined or not. However, the biggest alveoli are the first three from the tip of the mandible.

The posterior mandible (Fig. 3B, D) is represented by the last tooth row of the dentary, partial posterior splenial, the

surangular, the articular, and the angular. The dentary preserves the last three alveoli of the tooth row, with a more elliptical shape in comparison to the rest of the dentary. It contacts the anterior surangular posterolaterally, which makes a smooth anterodorsal concave transition, and still has a small portion of the splenial contacting it, posterior to the last alveolus. The posteriormost splenial has a subtriangular shape, anteriorly broken, that gets narrower posteroventrally, until it wedges and contacts the anterior angular. The splenial posterior surface forms part of the anterior and ventral limits of the internal mandibular fenestra.

The surangular is a short, rectangular bone that contributes to the posterodorsal border of the external mandibular fenestra. Dorsally, it has two dorsally projected processes: an anterior one, the coronoid process, near the contact with the dentary, and a posterior one, a “secondary coronoid process,” at the height of the posterior border of the mandibular fenestra. The ventral region of the surangular projects posterolaterally, displaying a smooth and deep shelf, from the height of the anterior coronoid process to the anterior glenoid, where it abruptly forms an almost vertical curvature to reach the glenoid. This deep shelf would have attached the jaw adductor musculature, as seen in other phytosaur mandibles (Hungerbühler, 1998; Mateus et al., 2014a). The edge of the surangular shelf makes a lateral crest that fuses with the articular. The surangular reaches below this lateral crest, meeting the angular in a concave and subhorizontal suture.

The prearticular-articular is here described as a single complex, as these bones are fully fused. The complex remains below the level of the dorsal edge of the surangular dorsal, and medially it expands anteriorly over the angular, contributing to the posteroventral surface of the internal mandibular fenestra. The glenoid facet is concave, wider than long, and anteromedially oriented. The lateral surface of the glenoid is straight, parallel to the surangular edge of the shaft. Medially, the glenoid facet expands anteromedially. The medial process of the prearticular-articular complex is a posteroventral extension of the glenoid facet. The anteroventral corner of the medial process is blunt and anteriorly reaches the middle part of the glenoid facet. The medial process and the internal face of the mandible create a deep, anteroventrally opened recess for the joint with the ventral ramus of the skull. The articular has a delicate process that projects dorsally in the posterior region of the internal glenoid. The apex of this process extends over the glenoid facet but stays below the surangular posterior process.

Laterally, the angular is anteriorly broken, and posteriorly projected into the retroarticular process. The dorsal surface of the angular forms part of the posteroventral border of the external mandibular fenestra. Medially, the angular contacts the posterior splenial, and dorsally it contacts the prearticular-articular complex and the posteroventral portion of the surangular. It only participates in the posteroventral border of the internal mandibular fenestra. Medially, the angular is concave and has a row of circular pits that begins near the posterior border of the fenestra, which extends posteriorly without reaching the articular. This feature could be for the attachment of mandibular musculature. The retroarticular process on the posteroventral edge of the angular is rounded and projects posteriorly.

The partial mandible NHMD-916730 (Fig. S1E, F) is poorly preserved, consisting of a thin portion of the dorsal region of the posterior mandible (posteriormost dentary, with its last tooth, the surangular, and the articular). The edges of the surangular and the articular are eroded, whereas the anterior and posterior projections of the surangular are recognizable and in a similar position in comparison with the holotype NHMD-916731, as the articular is also below the level of the dorsal edge of the surangular.

The angulars NHMD-916732 and NHMD-916733 (Fig. S1G, H) are both medially bowed and incomplete posteriorly. The

anterior edge has an anteriorly concave surface, in which the posterior splenial would contact, similar to the manner in which the splenial of the holotype NHMD-916731 wedges in the anterior portion of the angular. The ventral surface of NHMD-916733 is broken, which creates a convex shape, in contrast with NHMD-916732, which has a straight rectangular shape. The dorsal edges of both angulars are slightly concave. In comparison with the holotype, the anterior region of the dorsal edge of the angulars would participate in the ventral border of the internal mandibular fenestra, and the posterodorsal region would contact the surangular.

Teeth

A total of 62 isolated teeth were recovered, however only 45 are well preserved enough to warrant description (Figs. 5, S2; Table S3), along with the four teeth from the mandible NHMD-916721. Following the description and measurements (Fig. 4) from Hungerbühler (2000), the dentition displayed is “tripartite,” which differentiates the teeth in three groups: tip of the snout set (the first teeth of the premaxilla, before the diastema-like region), the premaxillary teeth (rest of the premaxilla, after the diastema-like region), and the maxillary teeth.

Tip of the Snout Set—Teeth NHMD-916734, NHMD-916735, and NHMD-916736 (Figs. 5A, S2A) have a conical shape, straight and almost circular in cross section. Their edges are smooth and without serrations.

Anterior Premaxilla Set—Teeth NHMD-916737 to NHMD-916752 (Figs. 5B–E, S2B). These teeth have a circular base in cross section, becoming more oval towards the apex. The teeth are strongly curved lingually, except for NHMD-916742, NHMD-916743, NHMD-916744, and NHMD-916752, which are straight. However, these four teeth are broken and are considered as part of the anterior premaxilla due to their lack of serration. A carina is present only in NHMD-916740, suggesting that NHMD-916738, NHMD-916739, and NHMD-916741 are more anteriorly located in the tooth row.

Posterior Premaxilla Set—Teeth from NHMD-916753 to NHMD-916759 (Figs. 5F–H, S2C) are complete crowns. They have a circular cross section, flattened lingually near the base, becoming asymmetrical with a D-shape, in contrast with the anterior premaxillary teeth. The teeth change from lingually curved (NHMD-916753, NHMD-916754, and NHMD-916757) to straight on both lingual and labial faces (NHMD-916755, NHMD-916756). Mesial and distal carinae are present and fully serrated along the entire height of the crown. Although some of the carinae are partially broken (NHMD-916753, NHMD-916754, and NHMD-916758), it can be assessed they are fully serrated. The serration starts to appear in the tooth row from the apex to the base (Hungerbühler, 2000), thus if these teeth have both mesial and distal basal carinae serrated, the crowns should as well.

Anterior Maxilla Set—Teeth from NHMD-916760 to NHMD-916768 (Figs. 5I, J, S2D) are broken crowns. Most of them, with the exception of NHMD-916765 and NHMD-916766, display a D-shape cross section, flattened to faintly curved lingually and convex labially. Although the apex is broken in some, all their crowns display carinae that are fully serrated medially and distally. These features are characteristic for anterior maxillary teeth posteriorly located in the tooth row (Hungerbühler, 2000, 2002). The teeth NHMD-916765, NHMD-916766, and NHMD-916767 have most of their carinae broken and with only partial remnants of the denticles, therefore their position is difficult to determine.

Posterior Maxilla Set—Nine teeth (from NHMD-916769 to NHMD-916778; Figs. 5K–N, S2E) preserve most of the crown, being labiolingually flattened, displaying a D-shape (NHMD-916772, NHMD-916774, NHMD-916776, NHMD-916777, and NHMD-916778) or oval-flattened cross section (NHMD-916769, NHMD-916770, NHMD-916771, NHMD-916773, and NHMD-916775). The distal and mesial carinae of the crowns are fully serrated, with a serration density (SD) between 3–4 denticles per millimeter. The oval-flattened cross section and the mesial and distal expanded carinae give the appearance of a

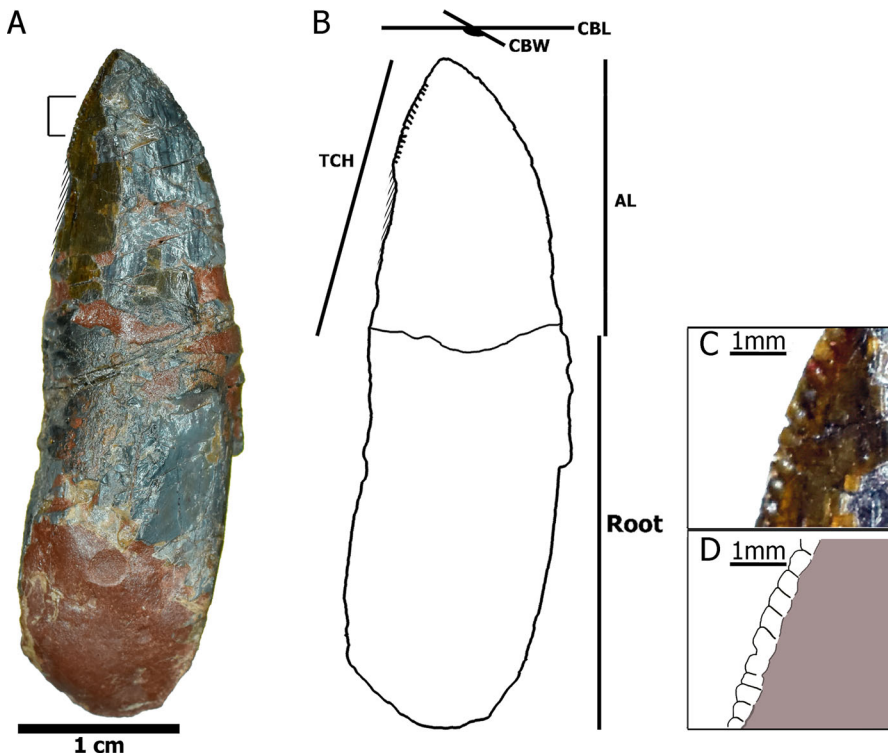


FIGURE 4. Measurements taken in teeth of *Myrstriosuchus alleroq*, sp. nov. **A**, tooth NHMD-916776; **B**, interpretative drawing and measurements based on NHMD-916776; **C**, closer look at the serration in the marked region of **A**; **D**, detail of the serration from closer look in **C**. **Abbreviations:** AL, apical length; CBL, length of crown-base; CBW, width of crown-base; TCH, tooth crown height.

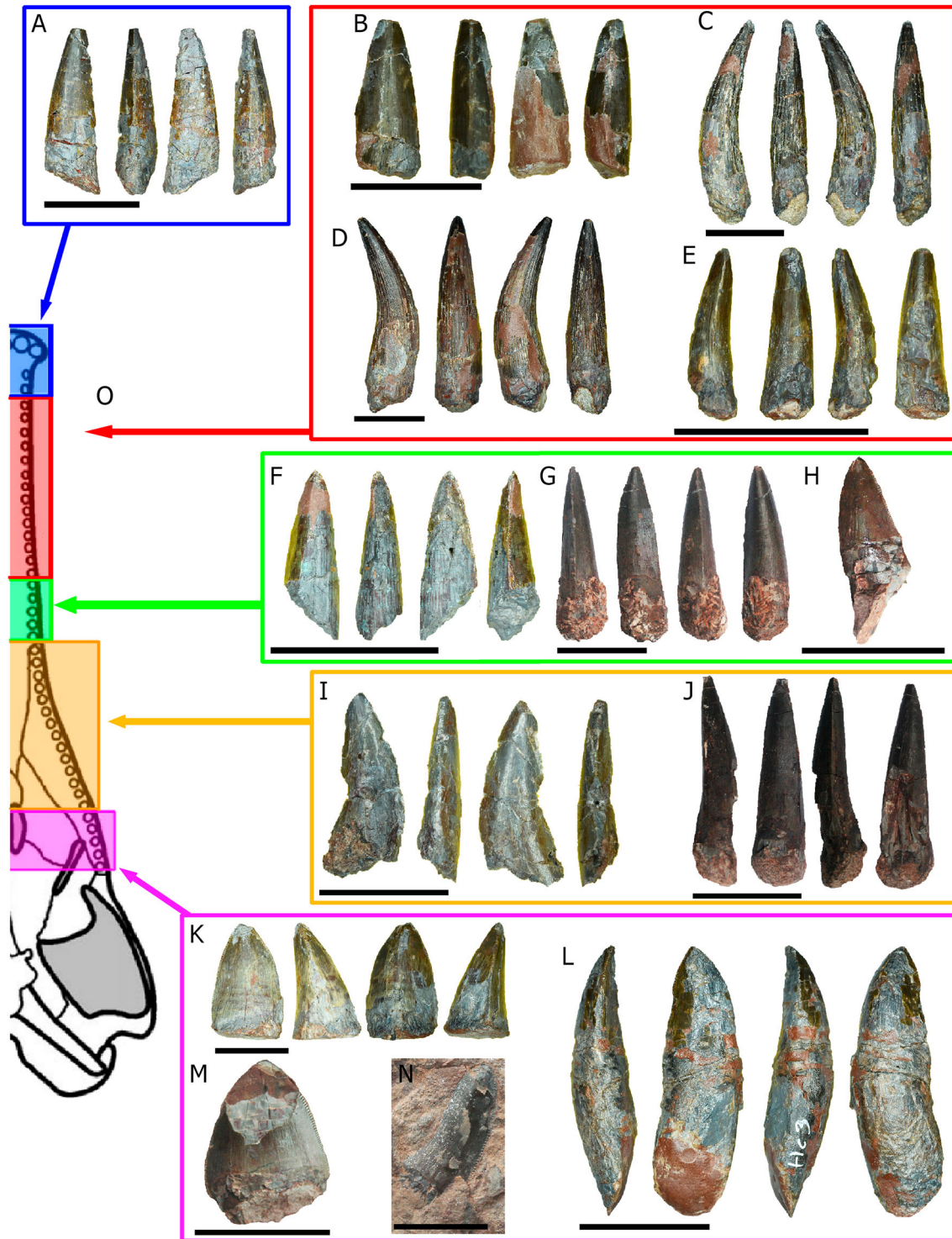


FIGURE 5. Teeth from *Mystriosuchus alleroq*. **A**, NHMD-916736; **B**, NHMD-916744; **C**, NHMD-916748; **D**, NHMD-916749; **E**, NHMD-916751; **F**, NHMD-916759; **G**, NHMD-916756; **H**, NHMD-916757; **I**, NHMD-916767; **J**, NHMD-916760; **K**, NHMD-916778; **L**, NHMD-916776; **M**, NHMD-916769; **N**, NHMD-916771; **O**, tooth regions are indicated by arrows and colors: blue—snout region (tooth A), red—anterior premaxilla region (teeth B–E), green—posterior premaxilla region (teeth F–H), orange—anterior maxilla region (teeth I–J), purple—posterior maxilla region (teeth K–N). Scale bars: **A–H**, **J**, **L–M** equal 2 cm; **I**, **K**, **N** equal 1 cm.

flattened tooth in the case of NHMD-916771 but this is less pronounced in both NHMD-916769 and NHMD-916770. Tooth NHMD-916772 has a morphology that resembles the anterior position more in comparison with the other three. However, it

is more flattened than the anterior maxillary teeth. Unfortunately, NHMD-916774, NHMD-916775, and NHMD-916777 have their borders partly broken and are badly preserved, so the serration density (SD) could not be measured.

Mandibular Set—The four dentary teeth found in NHMD-916731 can be related to their counterparts of the premaxilla and maxilla. The third and fourth dentary teeth are conical and faintly lingually curved, with a rounded cross section and the carinae displaying no serrations. The third tooth is smaller than the alveolus, probably being a new replacement tooth. These teeth are the counterparts of the “Tip of the snout” set. The eleventh tooth has its apex broken. It is, like the third tooth, smaller than the alveolus, which may mean it is also freshly replaced. However, it slightly curves lingually, and it is the counterpart of the “anterior premaxilla” set. The 36th tooth is more robust than the previous. It displays a D-shaped cross section and both carinae are fully serrated. This tooth can be considered the counterpart of the posterior “anterior maxilla” set.

Vertebrae

A total of 14 vertebrae from the cervical, dorsal, sacral, and caudal regions (Figs. 6, 7) have been collected (Table S4).

Cervical Vertebra—NHMD-916779 (Fig. 6B) is an almost complete neural arch, missing only the ventral region of the neural canal. It is regarded as a cervical vertebra because of the posteroventral orientation of the diapophysis (as seen in *Machaeroprotopus* cervical vertebra in Camp, 1930; Weems, 1979, 2018). Most phytosaurs had seven (*Machaeroprotopus*, Camp, 1930; *Mystriosuchus*, Gozzi & Renesto, 2003), or between seven and nine (“*Rutiodon*,” Romer, 1956) cervical vertebrae. Due to the large diapophysis of NHMD-916779, it represents one of the mid-posterior cervical vertebrae.

The neural spine is vertically oriented and transversely compressed. The anterior border of the neural spine is nearly vertical, whereas the posterior border is expanded posteriorly and fused to the postzygapophysis, giving the neural spine a triangular shape in lateral view. The prezygapophyses are anteriorly expanded making an open V-shaped outline facet, whereas the postzygapophyseal facets face ventrolaterally. The diapophysis is positioned ventral to the prezygapophyses and expands distally. The neural canal has a rounded shape.

Dorsal Vertebrae—Due to the height of the neural spine and the orientation of the diapophysis (Camp, 1930), we identify NHMD-916780 and NHMD-916781 as from the anterior or middle dorsal region, whereas NHMD-91682 and NHMD-916783 are from the posterior dorsal region. NHMD-916780 (Fig. 6C) is an almost complete neural arch, again missing only the ventral region of the neural canal. The neural spine is vertically directed, tilted to the right, and transversely compressed, with the anterior and posterior edges subparallel. The apex of the neural spine is transversely expanded, a common feature in dorsal vertebrae for the contacts with osteoderms (as seen in Camp, 1930; Gozzi & Renesto, 2003). The base of the neural spine has an anterior rounded process. The neural spine is taphonomically bent. The prezygapophyses are anteriorly expanded. The facets of the postzygapophyses form a widely open V-shape. Pre- and postzygapophyses project nearly horizontally. The neural canal remains are mostly complete, missing only the ventral region; with a round shape. The diapophyses project perpendicularly to the neural arch. The parapophyses are positioned on the anterior region of the neural arch, between the diapophyses and the prezygapophyses, and ventral to both.

NHMD-916781 (Fig. 6D) is an almost complete neural arch, and much like NHMD-916780, the zygapophyses are also damaged. However, it is still embedded within the matrix with only the lateral portion visible, with the lateral part of the neural canal broken. The neural spine is slightly tilted posteriorly, with the anterior and posterior margins subparallel, and transversely compressed. The apex of the neural spine is rounded and is not transversely expanded. The prezygapophyseal facets are nearly horizontal with dorsal orientation.

NHMD-916782 and NHMD-916783 (Fig. 6E, F) are the neural arch and the centrum isolated from the same vertebra, respectively. Both parts were found in association, and the suture limit can be seen in both. The neural spine NHMD-916782 is vertically directed, elliptical, and transversely compressed. The apex of the neural spine is convex, transversely expanded, and has a rectangular outline in anterior view. The prezygapophyses are anteriorly projected, with the facets dorsally oriented making an open U-shape (more open, with the central meeting point between the zygapophyses more curved than the open V-shape found in other vertebrae). The postzygapophyses are complete, shorter than the prezygapophyses, and ventrally oriented. The neural canal is round. The rib facet appears at the base of the neural arch, ventral to the neural canal. NHMD-916783 is slightly amphicoelous, with a rectangular-shape in lateral view, and sub-elliptical in both anterior and posterior views. The dorsal surface is partly broken, with contact facets remaining. The ventral surface is slightly concave.

Sacral Vertebrae—The two sacral vertebrae NHMD-916784 (Fig. 6G) are partially preserved and still embedded in the matrix. Their centra are fused, as well as their proximal diapophyses. The prezygapophyses and postzygapophyses are difficult to delimit due to preservation. The neural spines are separated and tilted posteriorly.

Caudal Vertebrae—The positions of the caudal vertebrae designated here are NHMD-916785 as the third (despite the missing centrum, the tubercle is less projected than in other caudal vertebrae), NHMD-916786 as fourth, NHMD-916787 as sixth, NHMD-916788 as seventh, NHMD-916789 as eighth, and NHMD-916790 as the tenth (due to missing chevron facets). The differences in size and morphology among the distal caudal vertebrae could mean that NHMD-916792 is in a more posterior position than NHMD-916791, and it should be one of the most distal caudal vertebrae.

NHMD-916785 (Fig. 7A) is a nearly complete neural arch, except for the left anterior neural canal portion and left prezygapophyses. The neural spine is vertically directed, blade-like in shape, and transversely compressed, with anterior and posterior margins subparallel. The apex of the neural spine is subhorizontal and slightly tilted anteriorly, with no transverse expansion. The anterior edge of the neural spine base has a slight anteriorly projecting and rounded process. The prezygapophyses project anteriorly, forming a deep curve with the neural spine. The postzygapophyses are almost complete, with a triangular shape and their facets facing almost horizontally.

NHMD-916787 (Fig. 7B) is a complete centrum and partial neural arch, preserving only the neural canal, postzygapophyses, and the uppermost portion of the neural spine. The partial neural spine is transversely compressed with the anterior and posterior margins subparallel. Its apex is subhorizontal and slightly tilted anteriorly with no transverse expansion. The postzygapophyses are robust and face ventrally, with slight taphonomic deformation to the right. The neural canal is cylindrical. The centrum is amphicoelous and larger posteriorly than anteriorly. The ribs are fused ventrally to the suture of the centrum and the neural arch. The ribs are slightly ventrally oriented.

NHMD-916790 (Fig. 7C) is a nearly complete vertebra, except for the posterolateral left part of the centrum and postzygapophyses. The neural spine is directed vertically, blade-like, and transversely compressed, with anterior and posterior margins subparallel. The apex of the neural spine is subhorizontal creating a rectangular outline in lateral view and is not expanded transversely. The anterior rim at the base of the neural spine forms a round tubercle that projects anteriorly. The prezygapophyseal facets have an open V-shape. The interprezygapophyseal vacuity is deep. The prezygapophyses only project slightly anterior to the anterior rim of

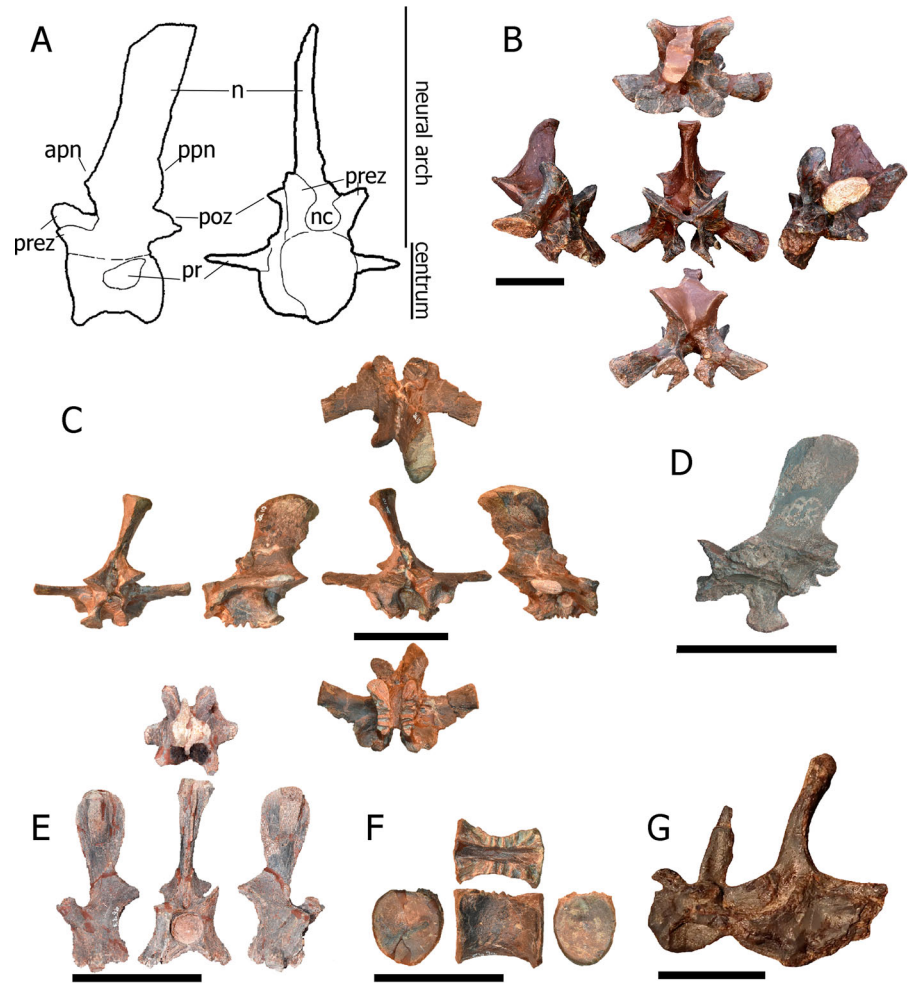


FIGURE 6. Vertebrae from *Myrstriosuchus alleroq*, sp. nov. **A**, morphological vertebrae characters found in *Myrstriosuchus alleroq*; **B**, cervical vertebra NHMD-916779 (dorsal, left, anterior, right, and posterior views); **C**, neural arch of dorsal vertebra NHMD-916780 (anterior, left, posterior, right, dorsal, and ventral views); **D**, dorsal vertebra NHMD-916781 (lateral view); **E**, dorsal vertebra neural spine NHMD-916782 (left, anterior, right, and dorsal views); **F**, dorsal vertebra centrum NHMD-916783 (anterior, lateral, posterior, and dorsal views); **G**, sacral vertebra NHMD-916784 (lateral view). **Abbreviations:** **apn**, anterior projection of the neural spine; **n**, neural spine; **nc**, neural canal; **poz**, postzygapophysis; **ppn**, posterior projection of the neural spine; **pr**, parapophyses; **prez**, prezygapophysis. Scale bars: **B**, **C**, **E–G** equal 5 cm; **D** equals 2 cm.

the centrum. The neural canal is round and three times the width of the pedicles. In the middle of the base of the neural spine, there is a discrete lateral vertical crest. The centrum is procoelous. The rib is broken with only the base preserved. The broken portion of the centrum reveals that the inner bone is mainly spongy with no visible pleurocoel. The fused neurocentral suture is located anterior to the rib. It is unclear if it runs ventrally or through the rib facet.

NHMD-916788 (Fig. 7D) is well preserved with a visible suture line between the neural arch and centrum. The neural spine is directed posterodorsally, transversely compressed, with subparallel anterior and posterior margins. The anterior half of the margin of the apex of the neural spine is angled, whereas the posterior half is horizontal. The apex of the neural spine is not expanded transversely. The base of the neural spine has anteriorly and posteriorly directed tubercles dorsal to the zygapophyses. The prezygapophyses have their facets dorsally oriented, making an open V-shape, whereas the postzygapophyses have their facets ventrally oriented. The interprezygapophyseal and interpostzygapophyseal vacuity are deep. The neural canal is rounded in outline. The centrum is amphicoelous, with a deep concave ventral surface. The ribs are fused between the suture of the centrum and the neural arch. The right rib is ventrally oriented, whereas the left rib is dorsally oriented due to taphonomic alterations. Both ribs are fused ventrally to the neurocentral suture.

NHMD-916786 (Fig. 7E) and NHMD-916789 (Fig. 7F) are nearly completely preserved. Their neural spines are directed vertically, slightly bowed, blade-like, and transversely compressed, with anterior and posterior margins subparallel. The prezygapophyses are robust and face dorsally, making an open V-shape. The prezygapophyses are anteriorly expanded, surpassing the centrum anterior margin, making a smooth 90° angle with the neural spine. The postzygapophyses are broken, face ventrally, and do not surpass the posterior margin of the centrum. The neural canal has a rounded shape anteriorly and an elliptical shape posteriorly. The centrum is amphicoelous, with a ventral concavity. The ribs are broken with only the base preserved between the suture of the neural arch and the centrum.

NHMD-916791 (Fig. 7G) is a broken caudal vertebra, with the neural spine preserved along with the left half of the posterior centrum. The neural spine is short, posteriorly located and posteriorly tilted, compressed transversely. The postzygapophyses are short and face ventrally. The neural canal is rounded in shape. The centrum is broken, with only the posterior portion remaining, but still procoelous. The left rib is short and perpendicular to the centrum, fused ventrally to the neural arch and the centrum suture.

NHMD-916792 (Fig. 7H) is a preserved small centrum. The centrum is procoelous, with the ventral surface concave. It possesses well preserved anterior and posterior articular surfaces for the chevrons.

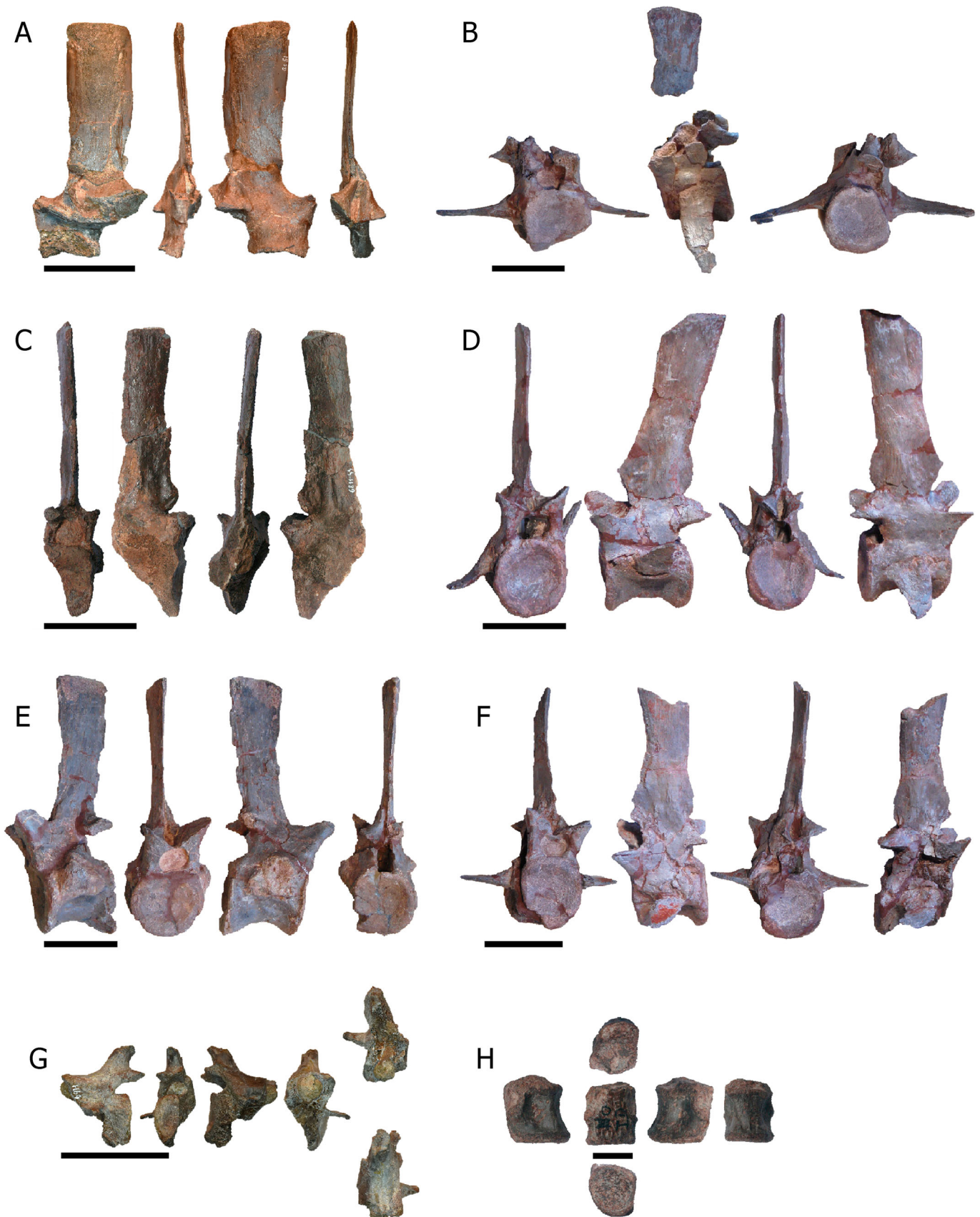


FIGURE 7. Caudal vertebrae from *Mystriosuchus alleroq*, sp. nov. **A**, NHMD-916785 (right, anterior, left, posterior views); **B**, NHMD-916787 (anterior, left, posterior views); **C**, NHMD-916790 (anterior, left, posterior, right views); **D**, NHMD-916788 (anterior, right, posterior, left views); **E**, NHMD-916786 (right, anterior, left, posterior views); **F**, NHMD-916789 (anterior, right, posterior, left views); **G**, neural arch NHMD-916791 (right, posterior, left, anterior, dorsal, and ventral views); **H**, distal vertebra NHMD-916792 (right, ventral, left, dorsal, anterior, and posterior views). Scale bars: **A–G** equal 5 cm, **H** equals 1 cm.

Cervical and Dorsal Ribs

A total of 40 ribs (Fig. S3; Table S5) were collected and can be divided into three morphotypes. Only the 23 most complete were measured.

The cervical ribs NHMD-91679 to NHMD-916798 (Fig. S3A–E) range from small and short, to long ribs, with dorsoventrally flattened, double headed proximal ends and a straight body.

The dorsal ribs NHMD-916799 to NHMD-916805 (Fig. S3F–L) are long and slender, with curvature ranging from straight to bowed. The proximal end is double headed (partly broken in NHMD-916799 and NHMD-916800), with the capitulum larger than the tuberculum. The proximal rib is dorsoventrally flattened, with a deep concave surface between the capitulum and the tuberculum. The rib becomes thicker distally, changing from a flat to a circular cross section that extends until the distal end. In the case of NHMD-916799 and NHMD-916803, the head displays smaller condyles, nearly identical in size. In NHMD-916800, the head is broken, missing the tuberculum.

Gastralia

The gastralia NHMD-916806 to NHMD-916815 (Fig. S3M–V) have a long and slender body shape, strongly curved with a prominent vertex in the middle of the body. The ends are broken and sharp in all of them, except for NHMD-916809.

Some partial distal ends (NHMD-916816 to NHMD-916823) and middle bowed parts (NHMD-916824 to NHMD-916832) cannot be identified into any of the previous rib types.

Appendicular Skeleton

Pectoral Girdle—A total of seven disarticulated bones referred to the pectoral girdle were recovered (Figs. 8A–E, S4A; Table S6).

The almost complete interclavicles (NHMD-916833, NHMD-916834, and NHMD-916835; Fig. 8A, B) are thin anteriorly, with a rhomboid outline in NHMD-916833 and a more triangular shape in NHMD-916834 due to the more laterally expanded lateral process. There are two median ridges on the ventral surface that run from the end to the anterior portion of the interclavicle body, almost reaching the end of the posterior body. The posterior body of the interclavicle, only preserved in NHMD-916835, is a thin sub-elliptical bone. In the anterior region, the contact with the interclavicle head is broken. There are two central ridges that run through the middle body. These ridges start as subparallel and separate distally.

The right clavicle NHMD-916836 (Fig. 8C) is short, flat, anteriorly bowed, and medially concave at its widest portion. Its anterior surface is straight and smooth, whereas the posterior surface has a concavity close to the medial end. It lacks the distal end and part of the medial end.

The partial left scapula NHMD-916839 (Fig. 8D) is subrectangular, posteriorly bowed, and has its distal end more posteriorly projected than its proximal end. The ventral surface of the distal end is triangular where it contacts the coracoid.

The right coracoid NHMD-916837 (Fig. 8E) has a convex blade-like shape that broadens posteriorly. The sub-elliptical glenoid process is oriented perpendicular to the blade. From the left coracoid NHMD-916838 (Fig. S4A), only the anterior portion of the blade region and the posterior portion of the glenoid process is preserved. The anterior portion of the blade-like region is thin with a sharp anterior edge. The glenoid process has a concavity that would contact the scapula.

Forelimbs—A total of six non-autopodial forelimb elements were collected (Figs. 8F, G, S4B–D; Table S7).

Complete right (NHMD-916843; Fig. 8F) and left humeri (NHMD-916841 and NHMD-916842; Fig. S4C, D) displays

robust and medially bowed diaphysis. Their proximal end is mediolaterally flattened with a rugose convex surface. The condyles are flat, the medial condyle being more expanded medially. The deltoid crest appears along the lateral margin of the anterior surface, almost reaching the middle portion of the body. The distal end is mediolaterally flattened, with broad condyle expansions. In contrast with the proximal surface, the distal surface is gently concave and soft. The radio-condylar groove is located above the laterodistal condyle and is ventrolaterally expanded.

The partial right ulnae (NHMD-916844 and NHMD-916845, Figs. 8G, S4B) are anteriorly bowed, mediolaterally flattened, and faintly medially concave. The proximal end is anteriorly broad, with a circular shape in lateral view. In NHMD-916844, it has a ventral expansion of the medial border, overlying the radius. On the anterior side, the olecranon has a smooth and poorly developed anterior concave surface. There is a laterally expanded sigmoidal relief along the midshaft. The distal end, complete in NHMD-916845, displays a concave ventral surface. The distal end is slightly bowed anteriorly, whereas the posterior surface projects posteriorly, displaying a pointed edge.

The right radius NHMD-916846 (Fig. 8G) is a straight subcylindrical bone, bowed medially but less than the ulna. The proximal end exhibits a flattened elliptical surface, more expanded medially than laterally. The distal end also exhibits a flattened surface, but the shape is more circular than the proximal surface.

Pelvic Girdle—The well-preserved left ischium NHMD-916840 (Fig. 9A) has a blade-like ventral process, mediolaterally flattened and posteriorly thinner, with the posterodorsal region thicker than the anteroventral. The dorsal rim is smooth.

Hindlimbs—One femur, one tibia, and one fibula were collected (Fig. 9B–D; Table S7). The left femur NHMD-916847 (Fig. 9B) displays a long, slender, sigmoidal shaft that is medially bowed. The femoral head is mediolaterally flattened, anteriorly expanded, and round, with a rugose convex surface. The fourth trochanter is positioned medially distal to the femoral head, in the proximal quarter of the shaft. The trochanter is long, representing nearly 21% of the femoral length, and has a rough projection medially. The medial and lateral condyles of the distal end are posteriorly oriented, with the medial condyle more expanded medially. The ventral surface is convex and smooth, larger in the medial condyle. The intercondylar grooves appear on both anterior and posterior surfaces but are deeper on the posterior surface.

The left tibia NHMD-916848 (Fig. 9D) has a robust, straight, medially bowed shape, with an oval cross section. The proximal end is anteriorly projected and more medially expanded than the distal end, with a smooth convex surface. The distal end is anteromedially expanded where it contacts the fibula.

The slender left fibula NHMD-916849 (Fig. 9C) is anteroposteriorly flattened, and the shaft shows a gentle sigmoid curvature. The proximal end has a smooth surface, and the lateral condyle is swollen in contrast to the medial. The diaphysis has an iliofibularis trochanter at the lateral part of the midshaft. The distal end has an ellipsoid smooth surface with a dorsal groove extending toward the middle diaphysis, and is flattened, in contrast with the proximal end.

Metapodia—A total of eight metapodial elements were recovered (Fig. S5; Table S7). The isolated metapodials from NHMD-916850 to NHMD-916857 are complete. None of the metapodials were articulated thus their exact position could not be determined.

The metapodia have rounded smooth proximal surfaces (flat in NHMD-916852 and NHMD-916857, dorsally concave in the others), whereas the distal surface is convex and flattened mediolaterally, making them subrectangular in anterior view. The ventral surface is smooth and straight in NHMD-916852, NHMD-916854, NHMD-916855, NHMD-916856, and NHMD-916857, and anteriorly concave in NHMD-916850, NHMD-916851, and NHMD-916853, whereas the dorsal surface is

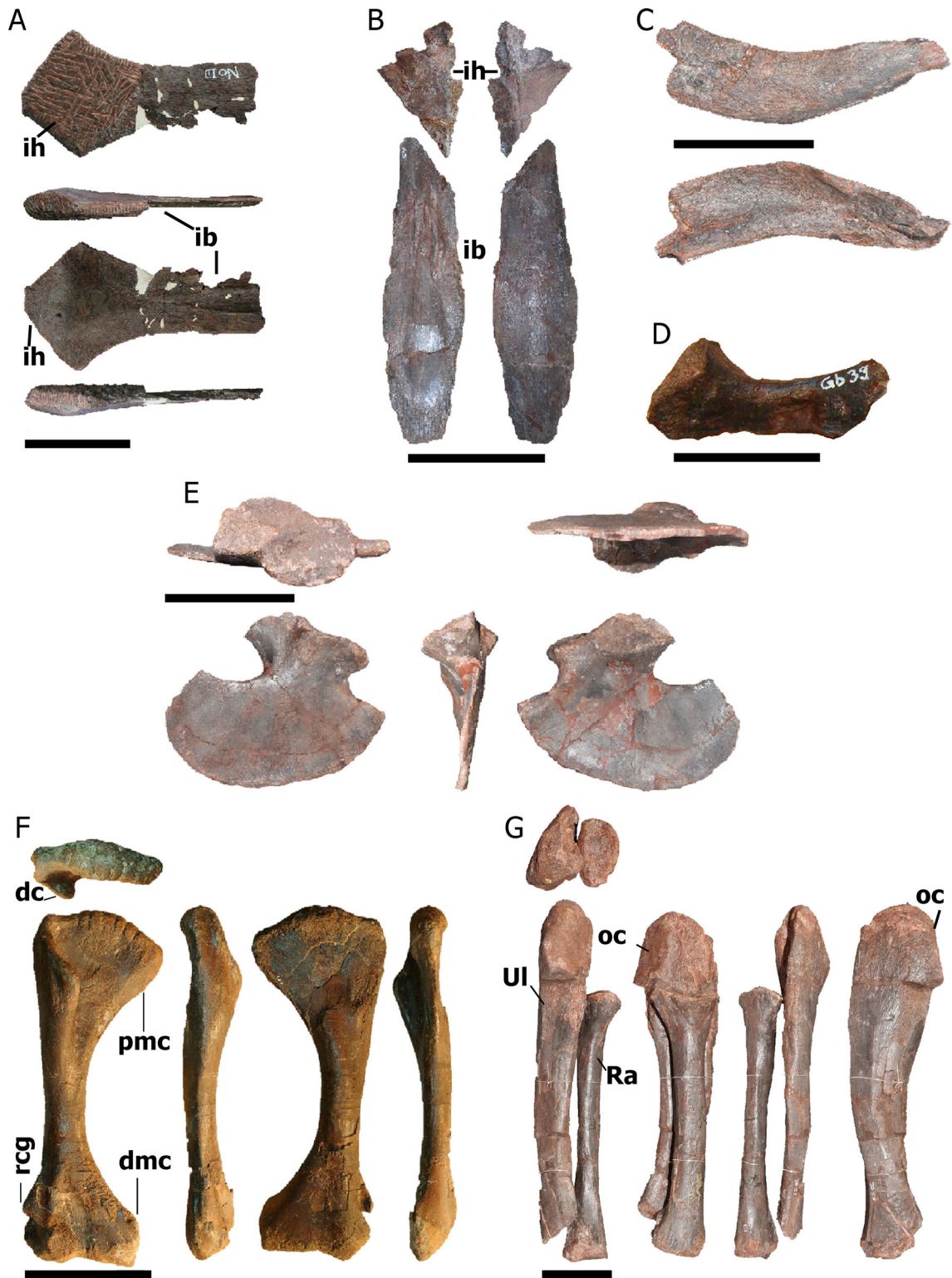


FIGURE 8. Pectoral girdle and forelimb bones of *Myrstriosuchus alleroq*, sp. nov. **A**, partial interclavicle NHMD-916833 (ventral, right, dorsal, and left views); **B**, interclavicle NHMD-916834 and NHMD-916835 (dorsal and ventral views); **C**, clavicle NHMD-916836 (anterior and posterior views); **D**, juvenile scapula NHMD-916839; **E**, right coracoid NHMD-916837 (lateral, posterior, medial, ventral, and dorsal views); **F**, right humerus NHMD-916843 (anterior, lateral, posterior, and medial views); **G**, right ulna and radius NHMD-916845 and NHMD-916846, respectively (anterior, medial, posterior, and lateral views). **Abbreviations:** **dc**, deltoid crest; **dmc**, distal medial condyle; **ib**, interclavicle body; **ih**, interclavicle head; **oc**, olecranon; **pmc**, proximal medial condyle; **Ra**, radius; **rcg**, radio-condylar groove; **Ul**, ulna. Scale bars **A**, **C**, **G** equal 4 cm; **B**, **E–F** equal 10 cm; **D** equals 2 cm.

slightly bowed. The anterior region is smaller than the posterior one, having a triangular shape in medial and lateral views. The body of the metapodia is constricted at the midshaft. The

anterolateral condyle is projected laterally, making the lateral surface appear more concave than the medial surface in the constricted area.



FIGURE 9. Pelvic girdle and hindlimb bones of *Mystriosuchus allerog*, sp. nov. **A**, left ischium NHMD-916840 (medial, anterior, and lateral views); **B**, left femur NHMD-916847 (anterior, medial, posterior, lateral views); **C**, left fibula NHMD-916849 (anterior, medial posterior, and lateral views); **D**, left tibia NHMD-916848 (posterior, medial, anterior, and lateral views). **Abbreviations:** **c**, condyle; **fc**, fibula contact; **fh**, femoral head; **gr**, groove; **p**, process; **tc**, trochanter. Scale bars: **A**, **D** equal 10 cm, **B–C** equal 4 cm.

Dermal Armor

A total of 19 osteoderms were collected (Fig. S6; Table S8). Phytosaur dermal armor remains are usually from the dorsal region (Lucas et al., 2002; Gozzi & Renesto, 2003; Zeigler et al., 2003a). Whereas the ventral armor is not often well-preserved (McGregor, 1906), the throat osteoderms or “gular shield” is typical for phytosaurs and different from other archosauriforms (Stocker & Butler, 2013; Holloway, 2018). Most of the isolated osteoderms found can be related to the lateral dorsal armor, due to the presence of pitting and strong sculpture on their dorsal surfaces, whereas in the “gular shield” pitting is not found (Stocker & Butler, 2013; Scheyer et al., 2014). We assign the osteoderms into different morphotypes, as they are isolated and not closely related to any vertebrae found. Additionally, some have lost their edges and are difficult to assign to a certain body region.

The first osteoderm morphotype (Fig. S6A–F) ranges from NHMD-916858 to NHMD-916863. These osteoderms have an almost longitudinal bilateral symmetry with a teardrop-shape and a mid-dorsal keel. The pitting appears in the dorsal region, in a rough convex surface, whereas the ventral region is smooth. The second osteoderm morphotype (Fig. S6G–M) ranges from NHMD-916864 to NHMD-916870. They display a dorsal keel near the medial edge, and a subcircular lateral expansion. The dorsal pitting and smooth ventral surface are similar to the previous morphotype. A third morphotype (Fig. S6N–P; NHMD-916871 to NHMD-916873) displays a central mid-dorsal keel, and strong lateral projections, with a subtriangular to subcircular shape with small spines along the edges. A fourth and final morphotype of the osteoderms (Fig. S6Q–S; NHMD-916874, NHMD-916875, and NHMD-916876) are ornamented with small interconnected ridges. These osteoderms are still embedded in matrix.

MICROANATOMICAL AND HISTOLOGICAL DESCRIPTION

The oval cross section of the right humerus NHMD-916843 has a central medullary cavity containing one large piece of endosteal bone that is surrounded by a broad perimedullary region grading into a remodeling zone (Fig. 10A). The cancellous medullary region consists of large irregularly formed erosion cavities intermixed towards its outer part with large secondary osteons. The medullary cavity comprises 21% of the mediolateral diameter of the bone, and the perimedullary region comprises 14.6%. The latter includes large erosion cavities and secondary osteons. In total approximately 64% of the cross section is occupied by primary periosteal bone. The entire cross section has a compactness of nearly 80%. The compactness of the periosteal region is roughly 94.6%, which is particularly high. Scattered secondary osteons occur beyond the perimedullary region up to the middle of the periosteal cortex.

The periosteal cortex can be divided into an inner and an outer portion. The primary tissue found in both parts is parallel-fibred bone tissue. The parallel-fibred bone is, however, deposited in different degrees of organization. In the inner cortex and in the zones, fibres are less organized than in the outer cortex and in the annuli (see below). In the outer cortex and in the annuli the parallel-fibred bone tissue is highly organized and may grade locally into lamellar bone (Fig. 10B–D). Neurovascular canal density in the inner cortex is moderate to low and in the outer cortex nearly avascular except for some local accumulation and/or alignments of neurovascular canals (Fig. 10A, B). Simple neurovascular canals and primary osteons occur (Fig. 10). Neurovascular canal size is small in general. Canal orientation is usually longitudinal, although some reticular and laminar ones occur. The periosteal cortex is regularly interrupted by growth marks

(see below, Fig. 10B). The bone tissue type can be summarized as lamellar zonal.

The moderate to low number of neurovascular canals and their absence in the outer cortex, as well as the dominance of parallel-fibred bone throughout the cortex indicates an average to low growth rate when compared with the growth rate of contemporaneous archosaurs (e.g., Ricqlès et al., 2003, 2008; Klein et al., 2017) but is comparable with that of phytosaur samples from Poland (Teschner et al., 2022). The inner cortex shows a higher number of neurovascular canals and a less organized tissue when compared with the nearly avascular and highly organized tissue of the outer cortex. Thus, a change in growth rate, i.e., slow down of growth rate during ontogeny is recorded.

The primary cortex is cyclically interrupted by growth marks in the form of alternating sequences of zones, annuli, and lines of arrested growth (LAGs), forming together annual growth cycles (Fig. 10B, C). However, the first two innermost preserved cycles each consist only of a broad zone and a thin annulus but a LAG is not developed (Fig. 10C). Zones consist of less organized and more highly vascularized tissue whereas the annuli are avascular and made of highly organized parallel-fibred bone or lamellar bone. Each of the following growth cycles end in a LAG, which is accompanied by additional rest lines (Fig. 10B). In the outer cortex the growth cycles become narrower as they are in the inner cortex, however there is no evidence of an outer circumferential layer *sensu* Ponton et al. (2004). Altogether 12 growth cycles can be counted (Fig. 10B). This is a minimal count because growth cycles of early ontogenetic stages are lost due to resorption. The number of lost cycles might be between 1 to 3, considering the space the medullary region occupies and the fact that growth cycles are broader in juvenile individuals (Klein and Sander, 2007). However, we refrain from equating this number with age in years because a more recent study has shown the ambiguity of growth cycle counts (Schucht et al., 2021). The tissue of the phytosaur from Greenland is very similar to what Butler et al. (2019) described for *Mystriosuchus steinbergeri* from the marine deposits from Austria. It differs from samples described by Ricqlès et al. (2003, 2008) by being more organized and not exhibiting juvenile tissue.

Contrary to the phytosaur samples from Poland (Teschner et al., 2022), the Greenland phytosaur shows LAGs, indicating regular pauses in growth, which indicates that the individual lived in a more seasonal climate. Heckert et al. (2021) described the histology of a pathological humerus from a phytosaur from North America. Aside from the pathological tissue, the osteohistology and microanatomy of that specimen are similar to that of the Greenland phytosaur.

DISCUSSION AND COMPARISONS

The phytosaurs from Greenland were found in a bonebed, consisting of at least four disarticulated individuals of different sizes. These individuals show no major intraspecific variation. There are no significant morphological differences in the bones that indicate more than one species. Apart from the morphological comparison and phylogenetic analysis of the Greenland phytosaur cranial material, the postcranial material was also compared with a variety of taxa. It is important to make postcranial comparisons alongside analyzing the new taxon in the matrix Jones and Butler (2018) because all of their characters are cranial. The matrices of Nesbitt (2011) and Ezcurra (2016) have 48% and 57% postcranial phylogenetic characters, but these are not focused on phytosaurs.

Dentition in phytosaurs has been used as a feature to differentiate early from later forms in the same family, based on character descriptions, whether “homodont” or “weakly-strong heterodonty” (Gregory, 1962; Hunt and Lucas, 1989; Long &

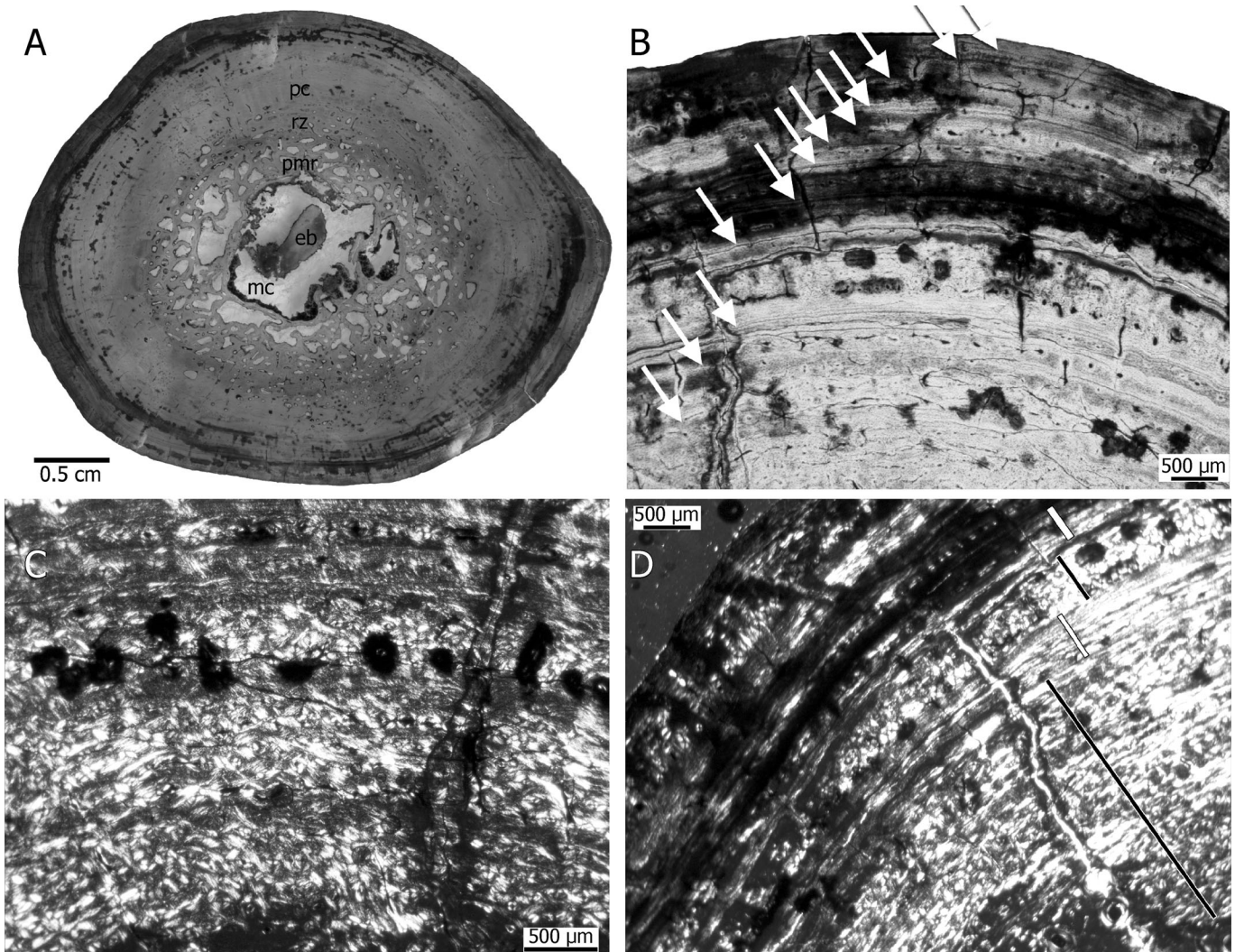


FIGURE 10. Bone histology of the right humerus NHMD-916843. **A**, cross section in normal light. Note the large perimedullary region and the compact cortex; **B**, annual growth cycle in the periosteal cortex marked by arrows in normal light; **C**, enlargement of the inner periosteal cortex displaying poorly organized parallel-fibred tissue in the inner and higher organized parallel-fibred tissue in the outer cortex in polarized light; **D**, enlargement of the outer cortex in polarized light. Black lines indicate zones and white lines annuli. **Abbreviations:** **eb**, endosteal bone; **mc**, medullary cavity; **pc**, primary cortex; **pmr**, perimedullary region, **rz**, remodeling zone.

Murry, 1995). The difference between “weakly” to “strong heterodonty” was not clearly explained until Hungerbühler (2000), who described in detail the dentition of the phytosaur *Nicrosaurus kapffi*. This has been used since then (Spielmann and Lucas, 2012; Datta et al., 2021) to help determine species, and even invoked to determine the feeding behavior (Hungerbühler, 2000; Hoffman et al., 2021). The different levels of heterodonty can differentiate phytosaurs based upon “tripartite dentition” (tip of the snout, premaxilla, and maxilla), or “bipartite dentition” (tip and post-tip of the snout; Hungerbühler, 2000). Mandibular teeth share the structure of their upper-jaw equivalents, but their morphology and transition between sets is less marked than the upper-jaw counterpart. However, the degree of heterodonty remains poorly studied in phytosaurs and is not used in phylogenetic nor morphometric research, in contrast to the situation for dinosaurs (e.g., Smith et al., 2005; Larson, 2008; Hendrickx & Mateus, 2014; Isasmendi et al., 2020).

The number of denticles is higher in teeth from the tip of the snout and anterior premaxilla of *N. kapffi*, whereas it is higher in the posterior premaxilla and the maxilla of *Myrstriosuchus*

alleroq. In comparison with *N. kapffi* from Hungerbühler (2000), *Myrstriosuchus alleroq* is here described as a phytosaur with a well-defined tripartite dentition.

In the rostrum NHMD-916722, in comparison with other phytosaurs and other archosauriforms, such as *Proterochampsia*, *Proterosuchus*, and *Eurparkeria* (Ewer, 1965; Rossmann et al., 2005; Dilkes & Arcucci, 2012), the premaxilla never reaches the antorbital fenestra. The suture between the premaxilla and maxilla is almost indiscernible in NHMD-916722. Only between tooth number 20 and 21 can a faint suture be observed. This suture extends dorsally and posteriorly while reaching the dorsal part, which may be the boundary between the premaxilla and maxilla. Following this interpretation, the tooth row would be divided, with almost half of them as premaxillary (20 premaxillary teeth) and the other maxillary (at least 16 maxillary, due to the maxilla being broken posteriorly). The subequal number of premaxillary and maxillary teeth can be seen in other phytosaurs such as *Angistorhinus grandis* (Mehl, 1915), *Parasuchus hislopi* (Chatterjee, 1978), or *Nicrosaurus kapffi* (Hungerbühler, 2000).

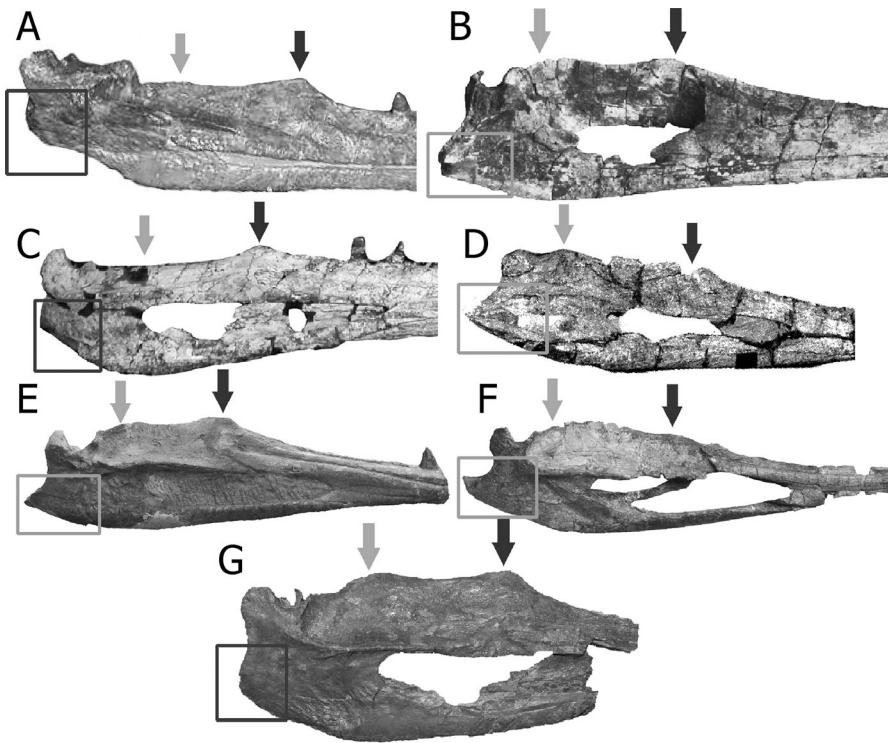


FIGURE 11. Position of the anterior (darker arrow) and posterior (gray arrow) dorsal projections of the surangular in different species of phytosaurs. Darker squares show the blunt-round feature of the retroarticular process, whereas the lighter squares show the pointed end of the same feature. **A**, *Smilosuchus* ‘*Leptosuchus*’ *gregorii* (modified from Irmis, 2005); **B**, *Protome batalaria* (modified from Stocker, 2012); **C**, *Machaeroprotopus* ‘*Pseudopalatus*’ *mccauleyi* (modified from Hunt et al., 2006); **D**, *Angistorhinus grandis* (modified from Lucas et al., 2002); **E**, *Mystriosuchus planirostris* SMNS 91574 (photograph by Octávio Mateus); **F**, Phytosauria indet. from Portugal (modified from Mateus et al., 2014a); **G**, *Mystriosuchus alleroq*, sp. nov., from Greenland (mirror image). Specimens are not to scale.

The premaxilla NHMD-916721 is similar in morphology and alveolar shape to that of *A. grandis* (Mehl, 1915) and *Protome batalaria* (Stocker, 2012), with a downturned terminal rosette in medial and lateral views. The terminal rosette is also downturned in *Mystriosuchus planirostris* and *M. westphali* (Hungerbühler, 2002), but in contrast with these, *M. alleroq* has a diastema after the teeth of the terminal rosette. The start of the interpremaxillary fossa from the fifth tooth is also found in *Machaeroprotopus lottorum* TTU-P10076 (Hungerbühler et al., 2012). However, the fossa of *Mystriosuchus alleroq* is not completely flattened posteriorly as it is slightly bowed dorsally towards the bottom of the maxilla.

In both jugals, the anterior edge has a smooth anterior concave surface, similar to the posterior and dorsal edges. This smooth concave surface could mean that the anterior region of the jugal was part of the antorbital fenestra, similar to other *Mystriosuchus* species, whereas the posterior ramus was part of the anteroventral lateral temporal fenestra (Hungerbühler, 2002; Butler et al., 2019). *M. alleroq* displays a long posterior ramus on the jugal, similar to *M. planirostris* or *M. westphali* (Hungerbühler, 2002), in contrast to the short posterior ramus of the jugal in *M. steinbergeri* (Butler et al., 2019).

The participation of the quadratojugal of *M. alleroq* (NHMD-916728) in the lateral temporal fenestra is greater than in *M. planirostris* or *M. westphali* (Hungerbühler, 2002), but less than in *M. steinbergeri* (Butler et al., 2019). It displays a similar morphology to *Ebrachosuchus neukami* (Butler et al., 2014), where the posterior ramus of the jugal projects below the anterior quadratojugal. In *M. alleroq* (Fig. 2F), the region where the jugal contacts is here indicated as the lateral ventral concavity of the anterior quadratojugal.

Hungerbühler indicated that phytosaurs display a jaw characterized, among other features, by a splenial that contributes to a large part of the symphysis but, in contrast, anteriorly reaches the mid-mandible, in contrast with other archosaurs (proterosuchids and sphenosuchids) that have splenials which almost reach the

tip of the mandible. However, the splenial is easily lost in dissociated material. In NHMD-916731, the splenial is not preserved and the dentary is highly distorted (Hungerbühler, 2001; Zeigler et al., 2003b; Heckert et al., 2013), so the anterior extent of the splenial is difficult to assess. In *Nicrosaurus kapffi* the splenial extends to the 15th–16th mandibular tooth (Hungerbühler, 2001), to the 17th–19th in *Brachysuchus* (Case, 1930), to the 19th–20th in *Machaeroprotopus mccauleyi* (Hunt et al., 2006), and to the 20th and 25th in the Western Texas phytosaur (UMMP 13534; Heckert et al., 2013). In *Mystriosuchus steinbergeri* it is difficult to assess, as the splenial is only recognizable in NHMW 1986/0024/0002 at around the 25th or 26th tooth position, with a slightly lower width than at the end of the symphysis (however it should reach a more anterior region; Butler et al., 2019). In *Mystriosuchus alleroq*, due to the fragmentary nature of the mandible, the splenial anteriormost position is unknown.

The surangular has two dorsally projected “coronoid processes”: one near the dentary and another near the articular. These dorsal projections have a similar position in NHMD-916730 and NHMD-916731, suggesting that even from different sizes, they could represent the same (or close) species. The anterior process projection of the surangular has been described by Hungerbühler (1998) as the coronoid process. However, the posterior projection here described as a ‘secondary coronoid process’ was never referenced. This ‘secondary coronoid process’ position and height has been compared with other phytosaur species (Fig. 11). Due to the lack of mandible material described and low resolution of some of the figures that are accessible, this first approach shows that the secondary coronoid process can be found, apart from *Mystriosuchus alleroq*, in *Nicrosaurus meyeri* (specimen of “*Belodon*” from Long and Murry, 1995:fig. 56), *Machaeroprotopus buceros* (Fig. 11C; from Zeigler et al., 2003b:fig. 7; and from Hunt et al., 2006), *Protome batalaria* (Fig. 11B; Stocker, 2012), and *Mystriosuchus planirostris* (Fig. 11E, specimen SMNS 13007, Stocker & Butler, 2013: fig. 6). Even though the mandibles of *Angistorhinus* have been

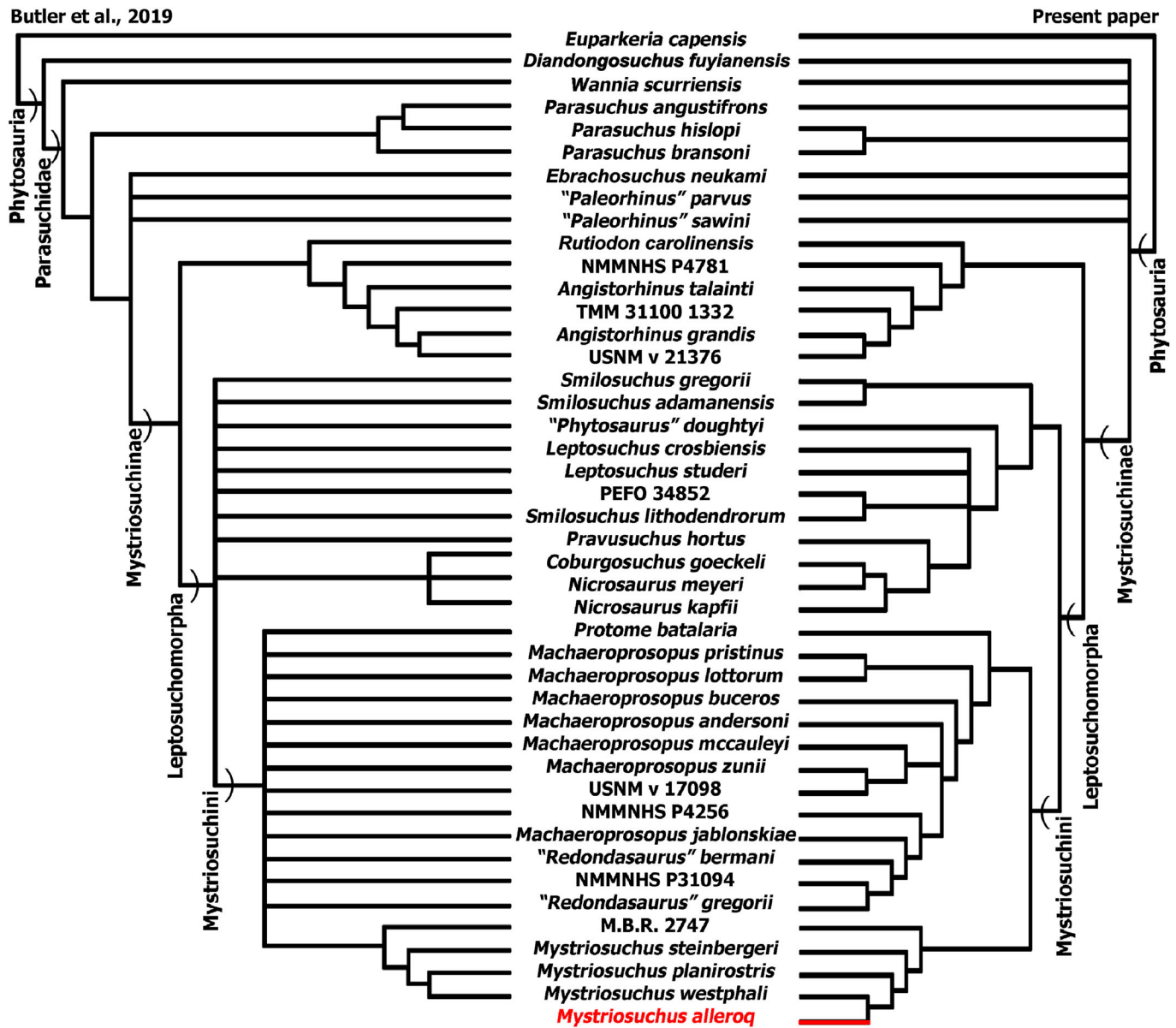


FIGURE 12. Relationships of Phytosauria based on Butler et al. (2019), left; and this paper, right.

found and depicted in Lucas et al. (1993, 2002), those mandibles have not been properly described, and the remains are difficult to compare from available figures (Lucas et al., 2002:fig. 2). However, *Angistorhinus* displays a subhorizontal dorsal border of the surangular, without significant projection of the coronoid (Lucas et al., 1993, 2002). *Smilosuchus gregorii* (Fig. 11A; Long & Murry, 1995; Irmis, 2005) has a strong horizontal surangular posterior to the coronoid process, in contrast with the two coronoid processes described above. The height, width, and shape of this secondary coronoid process is also different in the species that possess it. In *Machaeroprotopus buceros* and *Protome batalaria* both coronoid processes are at the same height; whereas in *Mystriosuchus* the coronoid is more dorsally projected than the secondary coronoid process, and in *Nicrosaurus meyeri*, the secondary coronoid process is taller. Even so, between the two species of *Mystriosuchus* described here, *M. planirostris* has its secondary coronoid process closer to the glenoid than in *M. alleroq*. While in *M. planirostris*, the transition from the

secondary coronoid process to the glenoid is gentle, in *M. alleroq* there is still a portion of the surangular between glenoid and the "secondary coronoid" that does not appear in *M. planirostris*, which is almost horizontal and separates both regions. Therefore, this feature could be a character developed in the Leptosuchomorpha, or in the Mystriosuchini clade with *Nicrosaurus* also developing it, as the non-mystriosuchini leptosuchomorphan *Smilosuchus gregorii* does not have this secondary coronoid process.

The prezygapophyses and postzygapophyses in the cervical vertebra NHMD-916779 are positioned dorsal to the neural canal (Lucas et al., 2002). However, the diapophyses of *Mystriosuchus alleroq* are located between the middle and ventral region of the neural canal. As seen in Camp (1930), the cervical vertebrae of *Machaeroprotopus* display a similar shape. The dorsal vertebrae of *Mystriosuchus alleroq* are similar to those of *Machaeroprotopus* (Camp, 1930), *Parasuchus* (Chatterjee, 1978), and *Angistorhinus* (Lucas et al., 2002), with the neural

spine apex transversely expanded, and the short square-shaped centrum amphicoelous, not keeled. The sacral vertebral neural spines are thinner than the ones from *Parasuchus* (Chatterjee, 1978) and *Angistorhinus* (Lucas et al., 2002).

The anterior caudal vertebrae of *Myrstriosuchus alleroq* (NHMD-916785 to NHMD-916790) possess, as seen in “*Rutiodon*” (Romer, 1956) and *Parasuchus* (Chatterjee, 1978), centra taller than wide. All caudal vertebrae from *Myrstriosuchus alleroq* share a feature that is not found either in cervical, dorsal, or sacral vertebrae, projections at the base of each neural spine (Figs. 6A, 7). All of them have anteriorly projected anterior tubercles at the base of the neural spine and some of them (NHMD-916788 and NHMD-916789) also have posterior tubercles. This feature is shared with other species of *Myrstriosuchus* (McGregor, 1906; Gozzi and Renesto, 2003; Renesto, 2008), but has not yet been found in other phytosaur taxa, possibly due to the lack of description of postcranial material (Gozzi & Renesto, 2003; Griffin et al., 2017).

The cervical ribs from *Myrstriosuchus alleroq* are similar to the ones described by Camp (1930) and Long and Murry (1995) for phytosaurs in general. In comparison with the almost complete specimen of *Myrstriosuchus planirostris* (Gozzi and Renesto, 2003), the cervical ribs of *M. alleroq* share the long and robust projected capitulum, almost transverse to the tuberculum. The dorsal ribs are longer and more curved (Camp, 1930), and similar in shape to those *M. planirostris* (Gozzi and Renesto, 2003). However, from *M. alleroq*, the dorsal rib NHMD-916805 could be indicated as a lumbar rib as it is flatter and straighter than the rest (as described in Camp, 1930), in contrast to *M. planirostris* (Gozzi and Renesto, 2003) in which the dorsal ribs have similar shape and without changes. The gastralia are, as in Gozzi and Renesto (2003), subcircular in cross section and rod-like.

In the pectoral girdle, the interclavicle NHMD-916833 has no notch in its anterior margin like the ones that appear in *Myrstriosuchus* (Gozzi and Renesto, 2003) or *Parasuchus* (Ezcurra, 2016), and the lateral process is very short in comparison with *Parasuchus* (Ezcurra, 2016). In contrast, the interclavicle (NHMD-916834, the anterior body, and NHMD-916835, the posterior body, of what looks like are the same interclavicle but broken) displays two middle ridges that appear in the anterior body that also were described by Camp (1930) for *Machaeropsopus*. However, the partial interclavicle NHMD-916834 is longer anteriorly, and appears to have the notch that NHMD-916833 lacks. It may represent an ontogenetic difference; there is generally a range of variation in the morphology of the genus *Myrstriosuchus* (Kimmig, 2009).

The tibia in *Myrstriosuchus alleroq* displays a more robust and stouter shape than *Machaeropsopus* (Camp, 1930). Also, the femur and fibula have preserved and well-developed trochanters for the attachment of muscles. Camp (1930) suggested that these trochanters could suggest the presence of a powerful tail for swimming, but also for walking adaptations. Butler et al. (2019) described *Myrstriosuchus steinbergeri* as a more marine species, in contrast to Camp (1930) for *Machaeropsopus* as a more terrestrial one.

The osteoderms of *Myrstriosuchus alleroq* were found isolated, which make it difficult to identify their relative position in the dermal armor. Gozzi and Renesto (2003) described only sub-elliptical and sub-pentagonal osteoderms for *M. planirostris*. However, those sub-elliptical osteoderms display a keel position similar to what we describe as the “first morphotype” (Fig. S6A–F), and the sub-pentagonal osteoderms have a medial keel similar to what here we describe as “the second morphotype” (Fig. S6G–M). If so, the “first morphotype” could be related to the two medial rows of the trunk region, whereas the “second morphotype” could be with the two lateral rows of the trunk.

PHYLOGENETIC POSITION

The analysis (phylogenetic information available as supplemental data S2, S3) recovered a total of 30 most parsimonious trees, with tree length of 349 steps and a Consistency Index (C.I.) of 0.390 and Retention Index (R.I.) of 0.697. The topology of the strict consensus is similar to the one presented by Jones and Butler (2018) and to Butler et al. (2019) when only discrete characters were used (i.e., without continuous characters; Fig. 12). The continuous characters were not included in this analysis because most of them refer to the narial region, the width of the skull, or a relation between two of them, which are missing in the new taxon.

Character 95 (degree of heterodonty) was introduced to better distinguish differences between early and later phytosaurs. As seen in Hungerbühler (2000), the three types of teeth in *Myrstriosuchus alleroq* are shared with *Nicrosaurus kapffi*, *Leptosuchus*, *Smilosuchus*, and *Machaeropsopus*, as more derived phytosaurs within the clade Leptosuchomorpha (Jones and Butler, 2018). However, the other two species of *Myrstriosuchus* (*planirostris* and *westphali*), the species *Nicrosaurus meyeri*, and *Redondasaurus* exhibit two sets of dentition. Dentition could imply difference in feeding ecology, and therefore, be an important character to differentiate closely related taxa, as it has been done with *Nicrosaurus kapffi* and *N. meyeri* (Hungerbühler, 2000; Hungerbühler and Hunt, 2000). The teeth attached in the mandible related to their isolated counterparts (snout, premaxilla, and maxilla) were used as the state “three set dentition” to score character 95.

There are two main differences in contrast to Butler et al. (2019) as a result of the addition of character 95: the relationships in the clade Leptosuchomorpha are better resolved, but the clades Phytosauria and Parasuchidae are collapsed into a polytomy that includes most of the early species (*Diandongosuchus fuyuanensis*, *Wannia scurriensis*, *Paleorhinus parvus*, *P. sawini*, *Parasuchus angustifrons*, and *Ebrachosuchus neukami*). This may be due to a lack of information about the degree of dentition in those species. The monophyletic *Angistorhinus* and “*Rutiodon*” has been recovered equal to the results of Jones and Butler (2018) and Butler et al. (2019), with “*Rutiodon*” *carolinensis* as the monospecific sister taxa of *Angistorhinus*. Jones and Butler (2018) indicated that the synonymy between both species was difficult to resolve, as the species *Brachysuchus megalodon* (Case, 1929) was not included in the matrix, which could be synonymous with *Angistorhinus*.

In the clade Leptosuchomorpha, the relationships are better resolved, creating a sister-taxon to Myrstriosuchini. It includes a new clade including *Pravusuchus hortus* + (*Nicrosaurus* + *Coburgosuchus goeckeli*), recovering a paraphyletic *Nicrosaurus*. And, whereas the relationships between *Smilosuchus* and *Leptosuchus* are better resolved, some polytomies cannot isolate *Leptosuchus* species from *Smilosuchus lithodendrorum*, PEFO 34852, and “*Phytosaurus*” *doughtyi*.

The clade Myrstriosuchini is divided into two subclades: first, the clade comprised of *Protome batalaria* + (*Machaeropsopus* + ‘*Redondasaurus*’ + NMMNHS P-31094), and a second clade composed by *Myrstriosuchus* and MB.R. 2747. Although there is a polytomy in the *Machaeropsopus* genus, the relationships between *Machaeropsopus* and “*Redondasaurus*” are better resolved. Previous analyses (Hungerbühler et al., 2012) suggested that “*Redondasaurus*” would be a synonym of the genus *Machaeropsopus*. Here, we recovered “*Redondasaurus*” in a clade with the unnamed species NMMNHS P31094, and *M. jablonskiae* as sister taxa. Therefore, here *Machaeropsopus* is recovered as a paraphyletic grouping. Finally, MB.R. 2747 appears (as in Jones and Butler, 2018) as the sister-taxon of *Myrstriosuchus* due to its lack of the diagnostic features: narrow and slit-like interpremaxillary fossa and interorbital nasal area cross section dorsally curved.

Here, the new taxon *Myrstriosuchus alleroq* is recovered within the genus *Myrstriosuchus* due to the possession of an interpremaxillary fossa both narrow and slit-like (Ch.2 = 2), nested closer to *M. westphali* and *M. planirostris* due to the proximal section of the postorbital descending process where the posterior border of the orbit remains thin until it meets the skull roof (Ch.88 = 1). *M. steinbergeri* also exhibits another state of the previous character (Ch.88 = 0), the postorbital descending process flares anteroposteriorly creating a wide triangular connection, along with two autapomorphies: (Ch.22 = 1) the antorbital fossa is present but with reduced lacrimal, jugal, and maxillary fossae in contact dorsally but not ventrally and (Ch.73 = 1) the suborbital foramen is elongated and slit-like. *Myrstriosuchus alleroq* is closer to *M. westphali* than to *M. planirostris* by sharing the absence of a narial crest (Ch.7 = 0).

Myrstriosuchus alleroq possesses two autapomorphies that differentiate it from *M. westphali*: an L-shaped quadratojugal with an anterior suture that trends anterodorsally (character 68 = 2); and a degree of heterodonty: tripartite upper dentition (character 95 = 2).

The shape of the rostrum in *M. alleroq* is more akin to that of *M. planirostris* or *M. steinbergeri*, straighter than that of *Myrstriosuchus westphali*, without the tubercle in the middle dorsal region of the premaxilla. However, *M. alleroq* has a smoother projection of the dorsal maxilla to meet the nasal, in contrast to the abrupt change (= “narial crest”; Jones and Butler, 2018) of *M. planirostris*.

The jugal of *Myrstriosuchus alleroq* displays a long posterior ramus, similar to that of *M. planirostris* or *M. westphali* (Hungerbühler, 2002), in contrast with the taller than longer jugal of *M. steinbergeri* (Butler et al., 2019). The quadratojugal of all species of phytosaurs have been described as having a subtriangular quadratojugal, except for *Euparkeria* and *Ebrachosuchus* (Jones and Butler, 2018). The contribution of the quadratojugal to the lateral temporal fenestra is very reduced to the posteroventral-most region in *M. planirostris* and *M. westphali* (Hungerbühler, 2002), whereas in *M. steinbergeri* the contribution is higher (almost the entire ventral and posteroventral borders; Butler et al., 2019). In *M. alleroq*, the contribution to the lateral temporal fenestra would be an intermediate position, as it contributes more than *M. planirostris* or *M. westphali*, but not as much as *M. steinbergeri*.

IMPLICATIONS

Myrstriosuchus alleroq contributes to a better understanding of the chronology and paleogeography of the Malmros Klint Formation. The chronological placement of *Myrstriosuchus alleroq* as mid-late Norian is consistent with other finds. European species of the genus *Myrstriosuchus* (*M. planirostris*, *M. westphali*, and *M. steinbergeri*) are restricted to the Alaunian and Sevatian (middle to late Norian; Hungerbühler, 2002; Butler et al., 2019), whereas the North American phytosaurs, such as *Angistorhinus* and *Machaeroprotopus*, are restricted to the Carnian–Norian (Lucas et al., 2002) and Norian–Rhaetian (Hunt and Lucas, 1993; Parker et al., 2012), respectively. The short range of the *Myrstriosuchus* clade is congruent with a Norian age for the Malmros Klint Formation at the Lepidopteris Elv locality.

Geographically, *Myrstriosuchus alleroq* reinforces the previous concept of the European faunal influence between East Greenland and Europe by the Late Triassic suggested by Jenkins et al. (1994) and Clemmensen et al. (1998), later supported by other researchers (Sulej et al., 2014; Marzola et al., 2017b). Moreover, *M. alleroq* is the northernmost *Myrstriosuchus* species found to date. During the Late Triassic, North America and Europe–Greenland were situated in different climatic zones that can be placed around the North Hadley Cell range. While the Colorado Plateau was in a transition zone between a humid and an arid climate belt, closer to the equator, Central Europe and Greenland

were situated in a more humid temperate climate belt farther to the north (Benton, 2016; Kent and Clemmensen, 2021). This could explain the separation between the North American and European–Greenland faunas at the end of the Triassic.

Due to size differences, we can distinguish a minimum of four individuals. The bones were disarticulated and only a few bones are repeated among individuals (humeri, premaxilla, and jugals), making identification of potential ontogenetic variation difficult. Suture closure over ontogeny has been studied in phytosaurs and crocodylians (Brochu, 1996; Irmis, 2007). Sutural fusion occurs in a posterior–anterior direction in crocodylians, so the postsacral vertebrae suture fuse in early ontogeny while presacral vertebrae suture fuse in late ontogeny (Irmis, 2007; Ikejiri, 2012). In the *M. alleroq* sample, presacral neurocentral junctions are unfused and caudal neurocentral junctions are fused. Only in the specimen NHMD-916788 (Fig. 7D) can a partial suture line be distinguished among the caudal vertebrae, suggesting that this specimen could be more juvenile than the others. Following Irmis (2007) and Ikejiri (2012), these findings suggest that the bigger *M. alleroq* individuals could be ‘more mature’ than the others, but not fully mature individuals. However, following Irmis (2007), further study of the sequence of phytosaur neurocentral suture closure is warranted.

ACKNOWLEDGMENTS

VLR was funded by the Fellowship 2021.06877.BD of the Fundação para a Ciência e Tecnologia. OM and VLR benefited from GeoBioTec-GeoBioSciences, GeoTechnologies and GeoEngineering NOVA [GeoBioCiências, GeoTecnologias e GeoEngenharias], grant UIDB/04035/2020 by the Fundação para a Ciência e Tecnologia. We gratefully acknowledge the support from Dronning Margrethes og Prins Henriks Fond, Arbejdsmarkedets Feriefond, Oticon Fonden, Knud Højgaard's Fond, Louis Petersens Legat, Det Obelske Familiefond, Ernst og Vibeke Husmans Fond, the Carlsberg Foundation, the Independent Research Fund Denmark, and Geocenter Møns Klint. The material was professionally prepared by V. Régent, as well as Museu de Lourinhã preparators, especially C. A. Tomás and M. Martinho. A special acknowledgment goes for N. Natrop who made the 2012 expedition possible. We are also grateful to N. R. Nielsen, E. Estrup and N. Natrop from the Geocenter Møns Klint for their participation in excavations, to M. Marzola for his previous work, to R. Butler and A. Jones for the discussions about the specimen in the various stages of the research, to V. Cheng for the English revision of the document, and to B. E. Kramer Lindow and the Natural History Museum of Denmark for facilitating access to the material.

ORCID

Víctor López-Rojas  <http://orcid.org/0000-0001-8996-7047>
 Lars B. Clemmensen  <http://orcid.org/0000-0002-3265-9307>
 Jesper Milàn  <http://orcid.org/0000-0002-9556-3177>
 Oliver Wings  <http://orcid.org/0000-0002-6482-6683>
 Nicole Klein  <http://orcid.org/0000-0003-3638-1194>
 Octávio Mateus  <http://orcid.org/0000-0003-1253-3616>

REFERENCES

- Agnoles, F. L., Mateus, O., Milàn, J., Marzola, M., Wings, O., Adolfsson, J. S., & Clemmensen, L. B. (2018). *Ceratodus tunuensis*, sp. nov., a new lungfish (Sarcopterygii, Dipnoi) from the Upper Triassic of central East Greenland. *Journal of Vertebrate Paleontology*, 38(2), e1439834. <https://doi.org/10.1080/02724634.2018.1439834>
- Andrews, S. D., Kelly, S. R., Braham, W., & Kaye, M. (2014). Climatic and eustatic controls on the development of a Late Triassic source rock in

- the Jameson Land Basin, East Greenland. *Journal of the Geological Society*, 171(5), 609–619. <https://doi.org/10.1144/jgs2013-075>
- Andrews, S. D., & Decou, A. (2019). The Triassic of Traill Ø and Geographical Society Ø, East Greenland: Implications for North Atlantic palaeogeography. *Geological Journal*, 54(4), 2124–2144. <https://doi.org/10.1002/gj.3287>
- Ballew, K. L. (1989). A phylogenetic analysis of Phytosauria (Reptilia: Archosauria) from the Late Triassic of the Western United States. In Lucas, S. G. and Hunt, A. P. (eds) *Dawn of the age of dinosaurs in the American Southwest*, 309–339. Albuquerque: New Mexico Museum of Natural History and Science.
- Barrett, P. M., Sciscio, L., Viglietti, P. A., Broderick, T. J., Suarez, C. A., Sharman, G. R., Jones, A. S., Munyikwa, D., Edwards, S. F., Chapelle, K. E. J., Dolman, K. N., Zondo, M., & Choiniere, J. N. (2020). The age of the Tashinga Formation (Karoo Supergroup) in the Mid-Zambezi Basin, Zimbabwe and the first phytosaur from sub-Saharan Africa. *Gondwana Research*, 81, 445–460. <https://doi.org/10.1016/j.gr.2019.12.008>
- Beccari, V., Mateus, O., Wings, O., Milàn, J., & Clemmensen, L. B. (2021). *Issi saaneq* gen. et sp. nov. –A New Sauropodomorph Dinosaur from the Late Triassic (Norian) of Jameson Land, Central East Greenland. *Diversity*, 13(11), 561. <https://doi.org/10.3390/d13110561>
- Benton, M. J. (2016). The Triassic. *Current Biology*, 26(23), R1214–R1218. <https://doi.org/10.1016/j.cub.2016.10.060>
- Brochu, C. A. (1996). Closure of neurocentral sutures during crocodylian ontogeny: Implications for maturity assessment in fossil archosaurs. *Journal of Vertebrate Paleontology*, 16(1), 49–62. <https://doi.org/10.1080/02724634.1996.10011283>
- Broom, R. (1913). Note on *Mesosuchus browni*, Watson, and on a new South African Triassic pseudosuchian (*Euparkeria capensis*). *Records of the Albany Museum*, 2, 394–396.
- Brusatte, S. L., Butler, R. J., Niedźwiedzki, G., Sulej, T., Bronowicz, R., & Satkūnas, J. (2013). First record of Mesozoic terrestrial vertebrates from Lithuania: phytosaurs (Diapsida: Archosauriformes) of probable Late Triassic age, with a review of phytosaur biogeography. *Geological Magazine*, 150(1), 110–122. <https://doi.org/10.1017/S0016756812000428>
- Buffetaut, E., & Ingavat, R. (1982). Phytosaur remains (Reptilia, Thecodontia) from the Upper Triassic of north-eastern Thailand. *Geobios*, 15(1), 7–17. [https://doi.org/10.1016/S0016-6995\(82\)80054-5](https://doi.org/10.1016/S0016-6995(82)80054-5)
- Buffetaut, E., Martin, M., & Monod, O. (1988). Phytosaur remains from the Cenger Formation of the Lycian Taurus (western Turkey): stratigraphical implications. *Geobios*, 21(2), 237–243. [https://doi.org/10.1016/S0016-6995\(88\)80020-2](https://doi.org/10.1016/S0016-6995(88)80020-2)
- Burmeister, K. C., Flynn, J. J., Parrish, J. M., & Wyss, A. R. (2006). Paleogeographic and biostratigraphic implications of new Early Mesozoic vertebrates from Poamay, central Morondava Basin, Madagascar. *New Mexico Museum of Natural History and Science Bulletin*, 37, 457–475.
- Butler, R. J., Rauhut, O. W., Stocker, M. R., & Bronowicz, R. (2014). (*Francosuchus*) *angustifrons* and *Ebrachosuchus neukami* from Germany, with implications for Late Triassic biochronology. *Zoological Journal of the Linnean Society*, 170(1), 155–208. <https://doi.org/10.1111/zoj.12094>
- Butler, R. J., Jones, A. S., Buffetaut, E., Mandl, G. W., Scheyer, T. M., & Schultz, O. (2019). Description and phylogenetic placement of a new marine species of phytosaur (Archosauriformes: Phytosauria) from the Late Triassic of Austria. *Zoological Journal of the Linnean Society*, 187(1), 198–228. <https://doi.org/10.1093/zoolinnean/zlz014>
- Camp, C. L. (1930). A study of the phytosaurs with description of new material from western North America. *Memoirs of the University of California*, 19, 174.
- Case, E. C. 1922. New reptiles and stegocephalians from the upper Triassic of western Texas. Carnegie Institution of Washington 321:1–84.
- Case, E. C. (1929). Description of the skull of a new form of phytosaur: with notes on the characters of described North American phytosaurs. *University of Michigan Studies, Memoirs of the University of Michigan Museums*, 2, 1–56.
- Case, E. C. (1930). On the lower jaw of *Brachysuchus megalodon*. *Contributions from the Museum of Paleontology, University of Michigan*, 3(8), 155–161.
- Chatterjee, S. (1978). A primitive parasuchid (phytosaur) reptile from the Upper Triassic Maleri Formation of India. *Paleontology*, 21(1), 83–127.
- Clemmensen, L. B., Kent, D. V., & Jenkins Jr, F. A. (1998). A Late Triassic lake system in East Greenland: facies, depositional cycles and palaeoclimate. *Palaeogeography, Palaeoclimatology, Palaeoecology*, 140(1–4), 135–159. [https://doi.org/10.1016/S0031-0182\(98\)00043-1](https://doi.org/10.1016/S0031-0182(98)00043-1)
- Clemmensen, L. B., Kent, D. V., Mau, M., Mateus, O., & Milàn, J. (2020). Triassic lithostratigraphy of the Jameson Land Basin (central East Greenland), with emphasis on the new Fleming Fjord Group. *Bulletin of the Geological Society of Denmark*, 68, 95–132. <https://doi.org/10.37570/bgsd-2020-68-05>
- Clemmensen, L. B., Milàn, J., Adolfsson, J. S., Estrup, E. J., Frobøse, N., Klein, N., Mateus, O., & Wings, O. (2016). The vertebrate-bearing Late Triassic Fleming Fjord Formation of central East Greenland revisited: stratigraphy, palaeoclimate and new palaeontological data. *Geological Society, London, Special Publications*, 434(1), 31–47. <https://doi.org/10.1144/SP434.3>
- Colbert, E. H. (1947). Studies of the phytosaurs *Machaeroprotopus* and *Rutiodon*. *Bulletin of the AMNH*, 88(2), 53–96.
- Cope, E. D. (1881). *Belodon* in New Mexico. *The American Naturalist*, 15, 922–23.
- Datta, D., S. Ray, & Bandyopadhyay, S. (2019). Cranial morphology of a new phytosaur (Diapsida, Archosauria) from the Upper Triassic of India: implications for phytosaur phylogeny and biostratigraphy. *Papers in Palaeontology*, 7(2), 675–708. <https://doi.org/10.1002/spp2.1292>
- Datta, D., Kumar, N., & Ray, S. (2021). Taxonomic identification of isolated phytosaur (Diapsida, Archosauria) teeth from the Upper Triassic of India and their significances. *Historical Biology*, 33(2), 272–282. <https://doi.org/10.1080/08912963.2019.1613652>
- Dilkes, D., & Arcucci, A. (2012). *Proterochampsia barrionuevoi* (Archosauriformes: Proterochampsia) from the Late Triassic (Carnian) of Argentina and a phylogenetic analysis of Proterochampsia. *Palaeontology*, 55(4), 853–885. <https://doi.org/10.1111/j.1475-4983.2012.01170.x>
- Dutuit, J. M. (1977). Description du crâne de *Angistorhinus talainti* n. sp: un nouveau Phytosaure du Trias atlasique marocain [Description of the skull of *Angistorhinus talainti* n. sp: a new Phytosaurus from the Moroccan Atlas Triassic]. *Muséum national d'histoire naturelle 3e série*, 66(486), 297–337.
- Dzik, J. (2001). A new *Paleorhinus* fauna in the Early Late Triassic of Poland. *Journal of Vertebrate Paleontology*, 21(3), 625–627. [https://doi.org/10.1671/0272-4634\(2001\)021\[0625:ANPFIT\]2.0.CO;2](https://doi.org/10.1671/0272-4634(2001)021[0625:ANPFIT]2.0.CO;2)
- Emmons, E. (1856). *Geological report on the Midland Counties of North Carolina*. George P. Putnam and Co., New York, XX, 352 pp.
- Ewer, R. F. (1965). The anatomy of the thecodont reptile *Euparkeria capensis* Broom. *Philosophical Transactions of the Royal Society of London. Series B. Biological Sciences*, 248(751), 379–435. <https://doi.org/10.1098/rstb.1965.0003>
- Ezcurra, M. D. (2016). The phylogenetic relationships of basal archosauriforms, with an emphasis on the systematics of proterosuchian archosauriforms. *PeerJ*, 4, e1778. <https://doi.org/10.7717/peerj.1778>
- Fraas, E., (1896). Die Schwäbischen Trias-Saurier nach dem Material der Kgl. Naturalien Sammlung in Stuttgart zusammengestellt. [The Swabian Triassic dinosaurs according to the material of the Royal Natural history collection compiled in Stuttgart] *Mitteilungen aus dem Königlichen Naturalienkabinett zu Stuttgart*, 5, 1–18.
- Fraas O. (1866). Vor der Sündfluth. Eine Geschichte der Urwelt [Before the flood. A history of the prehistoric world]. Stuttgart: Hoffmann'sche Verlagsbuchhandlung, 512 pp.
- Francillon-Vieillot, H., Buffrénil de, V., Castanet, J., Gérardudie, J., Sire, F. J., Zylberberg, I., & de Ricqlès, A. (1990). Microstructure and mineralization of vertebrate skeletal tissues. In: Carter, J. G. (ed.), *Skeletal biomineralization: Patterns, Processes and Evolutionary Trends*, 471–530. Van Norstrand Reinhold, New York.
- Goloboff, P. A., & Catalano, S. A. (2016). TnT version 1.5, including a full implementation of phylogenetic morphometrics. *Cladistics*, 32(3), 221–238. <https://doi.org/10.1111/cla.12160>
- Gozzi, E., & Renesto, S. (2003). A complete specimen of *Myrstriosuchus* (Reptilia, Phytosauria) from the Norian (Late Triassic) of Lombardy (Northern Italy). *Rivista Italiana di Paleontologia e Stratigrafia (Research in Paleontology and Stratigraphy)*, 109(3), 475–498.

- Gregory, J. T. (1962). The genera of phytosaurs. *American Journal of Science*, 260, 652–690.
- Gregory, J. T. (1969). Evolution und interkontinentale Beziehungen der Phytosauria (Reptilia). [Evolution and Intercontinental Relationships of Phytosauria (Reptilia)] *Paläontologische Zeitschrift*, 43(1–2), 37–51. <https://doi.org/10.1007/BF02987926>
- Griffin, C. T., Stefanic, C. M., Parker, W. G., Hungerbühler, A., & Stocker, M. R. (2017). Sacral anatomy of the phytosaur *Smilosuchus adamanensis*, with implications for pelvic girdle evolution among Archosauriformes. *Journal of Anatomy*, 231(6), 886–905. <https://doi.org/10.1111/joa.12681>
- Guarnieri, P., Brethes, A., & Rasmussen, T. M. (2017). Geometry and kinematics of the Triassic rift basin in Jameson Land (East Greenland). *Tectonics*, 36(4), 602–614. <https://doi.org/10.1002/2016TC004419>
- Heckert, A. B., Viner, T. C., & Carrano, M. T. (2021). A large, pathological skeleton of *Smilosuchus gregorii* (Archosauriformes: Phytosauria) from the Upper Triassic of Arizona, USA, with discussion of the paleobiological implications of paleopathology in fossil archosauromorphs. *Palaeontologia Electronica*, 24, 1–21. <https://doi.org/10.26879/1123>
- Heckert, A. B., Jenkins, H. S., Lucas, S. G., & Hunt, P. (2013). Mandibles of juvenile phytosaurs (Archosauria: Crurotarsi) from the Upper Triassic Chinle Group of Texas and New Mexico, USA. *New Mexico Museum of Natural History & Science Bulletin*, 61, 228–236.
- Hendrickx, C., & Mateus, O. (2014). *Torvosaurus gurneyi* n. sp., the Largest Terrestrial Predator from Europe, and a Proposed Terminology of the Maxilla Anatomy in Nonavian Theropods. *PLOS ONE*, 9(3), e88905. <https://doi.org/10.1371/journal.pone.0088905>
- Hendrickx, C., Mateus, O., & Araújo, R. (2015). A proposed terminology of theropod teeth (Dinosauria, Saurischia). *Journal of Vertebrate Paleontology*, 35(5), e982797. <https://doi.org/10.1080/02724634.2015.982797>
- Hoffman, D. K., Miller-Camp, J. A., & Heckert, A. B. (2021). Tooth enamel microstructure in North American Phytosauria (Diapsida: Archosauriformes): Implications for biogeography and ecology of a Late Triassic clade of crocodylian-like predators. *Palaeontologia Electronica*, 24(3), a32. <https://doi.org/10.26879/1162>
- Holloway, W. L. (2018). *Comparative Cranial Ecomorphology and Functional Morphology of Semiaquatic Faunivorous Crurotarsans* [Doctoral dissertation, Ohio University]. OhioLINK Electronic Theses and Dissertations Center. http://rave.ohiolink.edu/etdc/view?acc_num=ohiou1542230980102513
- von Huene, F. R. F. (1915). On reptiles of the New Mexican Trias in the Cope Collection. *Bulletin of the American Museum of Natural History*, 34, 485–507.
- Hungerbühler, A. (1998). Cranial anatomy and diversity of the Norian phytosaurs of Southwestern Germany [Doctoral dissertation, Faculty of Science, University of Bristol]. Explore Bristol Research, https://research-information.bris.ac.uk/ws/portalfiles/portal/34487322/265319_vol1.pdf
- Hungerbühler, A. (2000). Heterodonty in the European phytosaur *Nicrosaurus kapffi* and its implications for the taxonomic utility and functional morphology of phytosaur dentitions. *Journal of Vertebrate Paleontology*, 20(1), 31–48. [https://doi.org/10.1671/0272-4634\(2000\)020\[0031:HTEPN\]2.0.CO;2](https://doi.org/10.1671/0272-4634(2000)020[0031:HTEPN]2.0.CO;2)
- Hungerbühler, A. (2001). The status and phylogenetic relationships of “*Zanclodon*” *arenaceus*: the earliest known phytosaur? *Paläontologische Zeitschrift*, 75, 97–112. <https://doi.org/10.1007/BF03022600>
- Hungerbühler, A. (2002). The Late Triassic phytosaur *Myrstriosuchus westphali*, with a revision of the genus. *Palaeontology*, 45(2), 377–418. <https://doi.org/10.1111/1475-4983.00242>
- Hungerbühler, A., & Hunt, A. P. (2000). Two new phytosaur species (Archosauria, Crurotarsi) from the Upper Triassic of southwest Germany. *Neues Jahrbuch für Paläontologie Monatshefte*, 2000, 467–484. <https://doi.org/10.1127/njgpm/2000/2000/467>
- Hungerbühler, A., Mueller, B., Chatterjee, S., & Cunningham, D. P. (2012). Cranial anatomy of the Late Triassic phytosaur *Machaeroprotopus*, with the description of a new species from West Texas. *Earth and Environmental Science Transactions of the Royal Society of Edinburgh*, 103(3–4), 269–312. <https://doi.org/10.1017/S1755691013000364>
- Hunt, A. P. & Lucas, S. G. (1989). New genotype designations for the phytosaurs *Myrstriosuchus* and *Rutiodon* with a discussion of the taxonomic status of *Myrstriosuchus*, *Clepsysaurus* and *Rutiodon*. In Lucas, S.G. and Hunt, A.P. (eds.), Dawn of the Age of Dinosaurs in the American Southwest. *New Mexico Museum of Natural History, Albuquerque*. 340–348.
- Hunt, A. P., & Lucas, S. G. (1991). The *Paleorhinus* biochron and the correlation of the non-marine Upper Triassic of Pangaea. *Palaeontology*, 34(2), 487–501.
- Hunt, A. P., & Lucas, S. G. (1993). A new phytosaur (Reptilia: Archosauria) genus from the uppermost Triassic of the western United States and its biochronological significance. *New Mexico Museum of Natural History and Science Bulletin*, 3, 193–196.
- Hunt, A. P., Lucas, S. G., & Spielmann, J. A. (2006). Sexual dimorphism in a large brachyrostral phytosaur (Archosauria: Crurotarsi) from the Late Triassic of western North America. *New Mexico Museum of Natural History and Science Bulletin*, 37, 563–567.
- Ikejiri, T. (2012). Histology-based morphology of the neurocentral synchondrosis in *Alligator mississippiensis* (Archosauria, Crocodylia). *The Anatomical Record: Advances in Integrative Anatomy and Evolutionary Biology*, 295(1), 18–31.
- Irmis, R. B. (2005). The vertebrate fauna of the Upper Triassic Chinle Formation in Northern Arizona. In Guidebook to the Triassic Formations of the Colorado Plateau in northern Arizona: Geology, Paleontology, and History. Sterling J. Nesbitt, William G. Parker, and Randall B. Irmis (eds.) *Mesa Southwest Museum, Bulletin No. 9*, 26 pp.
- Irmis, R. B. (2007). Axial skeleton ontogeny in the Parasuchia (Archosauria: Pseudosuchia) and its implications for ontogenetic determination in archosaurs. *Journal of vertebrate Paleontology*, 27(2), 350–361.
- Isasmendi, E., Sáez-Benito, P., Torices, A., Navarro-Lorbés, P., & Pereda-Suberbiola, X. (2020). New insights about theropod palaeobiodiversity in the Iberian Peninsula and Europe: spinosaurid teeth (Theropoda, Megalosauroidea) from the Lower Cretaceous of La Rioja (Spain). *Cretaceous Research*, 116, 104600. <https://doi.org/10.1016/j.cretres.2020.104600>
- Jäger, G. F. von (1828) Über die fossile Reptilien, welche in Württemberg aufgefunden worden sind. [About the fossil reptiles found in Württemberg.] Stuttgart: Verlag der J. B. Metzler’schen Buchhandlung, p. 48.
- Jaekel, O. (1910). Über einen neuen Belodonten aus dem Buntsandstein von Bernburg. [About a new belodont from the red sandstone of Bernburg] *Sitzungsberichte der Gesellschaft naturforschender Freunde zu Berlin*, 5, 197–229.
- Jenkins, F. A., Shubin, N. H., Gates, S. M., & Padian, K. E. V. I. N. (2001). A diminutive pterosaur (Pterosauria: Eudimorphodontidae) from the Greenlandic Triassic. *Bulletin of the Museum of Comparative Zoology*, 156(1), 151–170.
- Jenkins, F. A. Jr., Shubin, N. H., Amarel, W. W., Gates, S. M., Schaff, C. R., Clemmensen, L. B., Downs, W. R., Davidson, A. R., Bonde, N. C., & Osbaeck, F. (1994). Late Triassic continental vertebrates and depositional environments of the Fleming Fjord Formation, Jameson Land, east Greenland. *Meddelelser om Grønland, Geoscience*, 32, 1–25.
- Jones, A. S., & Butler, R. J. (2018). A new phylogenetic analysis of Phytosauria (Archosauria: Pseudosuchia) with the application of continuous and geometric morphometric character coding. *PeerJ*, 6, e5901. <https://doi.org/10.7717/peerj.5901>
- Kent, D.V., & Clemmensen, L. B. (2021). Northward dispersal of dinosaurs from Gondwana to Greenland at the mid–Norian (215–212 Ma, Late Triassic) dip in atmospheric pCO₂. *Proceedings of the National Academy of Sciences*, 118(8), e2020778118. <https://doi.org/10.1073/pnas.2020778118>
- Kent, D. V., & Tauxe, L. (2005). Corrected Late Triassic latitudes for continents adjacent to the North Atlantic. *Science*, 307, 240–244. <https://doi.org/10.1126/science.1105826>
- Kent, D. V., Santi Malnis, P., Colombi, C. E., Alcober, O. A., & Martínez, R. N. (2014). Age constraints on the dispersal of dinosaurs in the Late Triassic from magnetochronology of the Los Colorados Formation (Argentina). *Proceedings of the National Academy of Sciences*, 111(22), 7958–7963. <https://doi.org/10.1073/pnas.1402369111>
- Kimmig, J. (2009). Functional morphology and systematic palaeontology of the Phytosauria (Archosauria; Crurotarsi) and the development

- of their Late Triassic habitats [Msc dissertation, Department of Life Sciences and the Natural History Museum, Imperial College London]. 118 pp.
- Kimmig, J., & Arp, G. (2010). Phytosaur remains from the Norian Arnstadt Formation (Leine Valley, Germany), with reference to European phytosaur habitats. *Paleodiversity*, 3, 215–224.
- Kischlat, E. E. (2022). Phytosaurian nomenclature: Parasuchia, Belodontia or Phytosauria?. *Revista Brasileira de Paleontologia*, 25(1), 38–50. <https://doi.org/10.4072/rbp.2022.1.03>
- Kischlat, E. E., & Lucas, S. G. (2003). A phytosaur from the Upper Triassic of Brazil. *Journal of Vertebrate Paleontology*, 23(2), 464–467. [https://doi.org/10.1671/0272-4634\(2003\)023\[0464:APFTUT\]2.0.CO;2](https://doi.org/10.1671/0272-4634(2003)023[0464:APFTUT]2.0.CO;2)
- Klein, N., & Sander, P. M. (2007). Bone histology and growth of the prosauropod *Plateosaurus engelhardti* Meyer, 1837 from the Norian bonebed of Trossingen (Germany) and Frick (Switzerland). *Special Papers in Paleontology*, 77, 169–206.
- Klein, N., Foeth, Ch., & Schoch, R. R. (2017). Preliminary observations on the bone histology of the Middle Triassic pseudosuchian archosaur *Batrachotomus kupferzellensis* reveal fast growth with laminar fibrolamellar bone tissue. *Journal of Vertebrate Paleontology*, 37(4), e1333121. DOI: [10.1080/02724634.2017.1333121](https://doi.org/10.1080/02724634.2017.1333121)
- Klein, H., Milàn, J., Clemmensen, L. B., Frobøse, N., Mateus, O., Klein, N., Adolfsen, J. S., Estruo, E., & Wings, O. (2016). Archosaur footprints (cf. Brachychirotherium) with unusual morphology from the Upper Triassic Fleming Fjord formation (Norian–raetian) of East Greenland. *Geological Society, London, Special Publications*, 434(1), 71–85. <https://doi.org/10.1144/SP434.1>
- Kuhn, O. (1936). Weitere Parasuchier und Labyrinthodonten aus dem Blasensandstein des mittleren Keuper von Ebrach. [More parasuchians and labyrinthodonts from the bubble sandstone of the middle Keuper from Ebrach] *Palaeontographica Abteilung A*, 83, 61–98.
- Lagnaoui, A., Klein, H., Saber, H., Fekkek, A., Belahmira, A., & Schneider, J. W. (2016). New discoveries of archosaur and other tetrapod footprints from the Timezgadiouine Formation (Irohalene Member, Upper Triassic) of the Argana Basin, western High Atlas, Morocco—Ichnotaxonomic implications. *Palaeogeography, Palaeoclimatology, Palaeoecology*, 453, 1–9. <https://doi.org/10.1016/j.palaeo.2016.03.022>
- Lallensack, J. N., Klein, H., Milàn, J., Wings, O., Mateus, O., & Clemmensen, L. B. (2017). Sauropodomorph dinosaur trackways from the Fleming Fjord Formation of East Greenland: evidence for Late Triassic sauropods. *Acta Palaeontologica Polonica*, 62(4), 833–843. <https://doi.org/10.4202/app.00374.2017>
- Larson, D. W. (2008). Diversity and variation of theropod dinosaur teeth from the uppermost Santonian Milk River Formation (Upper Cretaceous), Alberta: a quantitative method supporting identification of the oldest dinosaur tooth assemblage in Canada. *Canadian Journal of Earth Sciences*, 45(12), 1455–1468. <https://doi.org/10.1139/E08-070>
- Li, C., Wu, X. C., Zhao, L. J., Sato, T., & Wang, L. T. (2012). A new archosaur (Diapsida, Archosauriformes) from the marine Triassic of China. *Journal of Vertebrate Paleontology*, 32(5), 1064–1081. <https://doi.org/10.1080/02724634.2012.694383>
- Long, R. A., and P. A. Murry. 1995. Late Triassic (Carnian and Norian) Tetrapods from the Southwestern United States. *Bulletin of the New Mexico Museum of Natural History and Science*, 4, 254.
- Lucas, S. G., Hunt, A. P., & Kahle, R. O. B. E. R. T. (1993). Late Triassic vertebrates from the Dockum Formation near Otis Chalk, Howard County, Texas. *New Mexico Geological Society Guidebook*, 44, 237–244.
- Lucas, S. G., Heckert, A. B., & Kahle, R. (2002). Postcranial anatomy of *Angistorhinus*, a Late Triassic phytosaur from West Texas. *Upper Triassic Stratigraphy and Paleontology, New Mexico Museum of Natural History and Science Bulletin*, 21, 157–164.
- Lydekker, R. (1885). The Reptilia and Amphibia from the Maleri and Denwa Groups. *Palaeontologia Indica* 4, 1(5), 1–38.
- Maisch, M. W., & Kapitzke, M. (2010). A presumably marine phytosaur (Reptilia: Archosauria) from the pre-planorbis beds (Hettangian) of England. *Neues Jahrbuch für Geologie und Paläontologie–Abhandlungen*, 257(3), 373–379. <https://doi.org/10.1127/0077-7749/2010/0076>
- Marzola, M. (2019). The Late Triassic vertebrate fauna of the Jameson Land Basin, East Greenland: description, phylogeny, and palaeoenvironmental implications. [Doctoral dissertation, Faculdade de Ciências e Tecnologia, Universidade Nova de Lisboa]. 260 pp.
- Marzola, M., Mateus, O., Milàn, J., & Clemmensen, L. B. (2018). A review of Palaeozoic and Mesozoic tetrapods from Greenland. *Bulletin of the Geological Society of Denmark*, 66, 21–46. <https://doi.org/10.37570/bgsd-2018-66-02>
- Marzola, M., Mateus, O., Milàn, J., & Clemmensen, L. B. (2017a). The 2016 Dinosaur Expedition to the Late Triassic of the Jameson Land Basin, East Greenland 249–253. In: Barrios de Pedro, S.; Blanco Moreno, C.; de Celis, A., Colmenar, J.; Cuesta, E.; García-Martínez, D.; Gascó, F.; Jacinto, A.; Malafaia, E.; Martín Jiménez, M.; de Miguel Chaves, C.; Mocho, P.; Pais V.; Páramo Blázquez, A.; Pereira, S.; Serrano Martínez, A.; Vidal, D. (Eds), *A Glimpse of the Past. Abstract Book of the XV Encuentro de Jóvenes Investigadores en Paleontología/XV Encontro de Jovens Investigadores em Paleontologia*, Lisboa.
- Marzola, M., Mateus, O., Shubin, N. H., & Clemmensen, L. B. (2017b). *Cyclotosaurus naraserluki*, sp. nov., a new Late Triassic cycloosaurid (Amphibia, Temnospondyli) from the Fleming Fjord Formation of the Jameson Basin (East Greenland). *Journal of Vertebrate Paleontology*, 37(2), e1303501. <https://doi.org/10.1080/02724634.2017.1303501>
- Mateus, O., Butler, R. J., Brusatte, S. L., Whiteside, J. H., & Steyer, J. S. (2014a). The first phytosaur (Diapsida, Archosauriformes) from the Late Triassic of the Iberian Peninsula. *Journal of Vertebrate Paleontology*, 34(4), 970–975. <https://doi.org/10.1080/02724634.2014.840310>
- Mateus, O., Clemmensen, L. B., Klein, N., Wings, O., Frobøse, N., Milàn, J., Adolfsen, J. S., & Estrup, E. (2014b). The Late Triassic of Jameson Land revisited: new vertebrate findings and the first phytosaur from Greenland. In: Maxwell, E. and Miller-Camp, J. (eds) *Society of Vertebrate Paleontology, 74th Meeting, Program and Abstracts*, 5–8 November 2014, Berlin, Germany. Society of Vertebrate Paleontology, Bethesda, MD, 182 pp.
- Mau, M., Kent, D. V., & Clemmensen, L. B. (2022). Planetary chaos and inverted climate phasing in the Late Triassic of Greenland. *Proceedings of the National Academy of Sciences*, 119(17), e2118696119. <https://doi.org/10.1073/pnas.2118696119>
- McGregor, J. H. (1906). The Phytosauria, with special reference to *Mystriosuchus* and *Rhytidodon*. *Memoirs of the American Museum of Natural History*, 9, 27–100.
- Mehl, M. G. (1913). *Angistorhinus*, a new genus of Phytosauria from the Trias of Wyoming. *The Journal of Geology*, 21(2), 186–191.
- Mehl, M. G. (1915). The Phytosauria of the Trias. *The Journal of Geology*, 23(2), 129–165.
- Mehl, M. G. (1928a). *Pseudopalatus pristinus*, a new genus and species of phytosaurs from Arizona. *University of Missouri Studies*, 3, 1–22.
- Mehl, M. G. (1928b). The Phytosauria of the Wyoming Triassic. Denison University Bulletin, *Journal of the Scientific Laboratories*, 23, 141–172.
- Milàn, J., Mateus, O., Mau, M., Rudra, A., Sanei, H., & Clemmensen, L. B. (2021). A possible phytosaurian (Archosauria, pseudosuchia) coprolite from the late triassic fleming fjord group of jameson land, central east Greenland. *Bulletin of the Geological Society of Denmark*, 69, 71–80. <https://doi.org/10.37570/bgsd-2021-69-05>
- Nesbitt, S. J. (2011). The early evolution of archosaurs: relationships and the origin of major clades. *Bulletin of the American Museum of Natural History*, 352, 1–292.
- Niedzwiedzki, G., & Sulej, T. (2020). Theropod dinosaur fossils from the Gipsdalen and Flemming fjord formations (Carnian–Norian, Upper Triassic), East Greenland. *Abstracts and Proceedings of the Geological Society of Norway The 34th Nordic Geological Winter Meeting January 8th–10th*. 2020, Oslo, Norway, 151 pp.
- Nøtvedt, A., Johannessen, E. P., & Surllyk, F. (2008). The mesozoic of western Scandinavia and East Greenland. *Episodes Journal of International Geoscience*, 31(1), 59–65.
- Owen, R. (1859). On the orders of fossil and recent Reptilia and their distribution in time. *Report of the British Association for the Advancement of Science*, 29, 153–166.
- Parker, W. G., Hungerbühler, A., & Martz, J. W. (2012). The taxonomic status of the phytosaurs (Archosauriformes) *Machaeropsopos* and *Pseudopalatus* from the Late Triassic of the western United

- States. *Earth and Environmental Science Transactions of the Royal Society of Edinburgh*, 103(3–4), 265–268. <https://doi.org/10.1017/S1755691013000339>
- Ponton, F., Elżanowski, A., Castanet, J., Chinsamy, A., De Margerie, E., De Ricqlès, A., & Cubo, J. (2004). Variation of the outer circumferential layer in the limb bones of birds. *Acta Ornithologica*, 39(2), 137–140.
- Renesto, S. (2008). Remains of a juvenile phytosaur from the Late Triassic of northern Italy. *Rivista Italiana di Paleontologia e Stratigrafia*, 114(1), 155–160.
- Ricqlès, A. J. de, Padian, K., & Horner, J. R. (2003, April). On the bone histology of some Triassic pseudosuchian archosaurs and related taxa. *Annales de Paléontologie*, 89(2), 67–101.
- Ricqlès, A. J. de, Padian, K., Knoll, F., & Horner, J. R. (2008, April). On the origin of high growth rates in archosaurs and their ancient relatives: complementary histological studies on Triassic archosauriforms and the problem of a “phylogenetic signal” in bone histology. *Annales de Paléontologie*, 94(2), 57–76.
- Romer, A. S. (1956). *Osteology of the Reptiles*. Chapter 6: The axial skeleton. University of Chicago Press, Chicago, 772pp.
- Rossmann, T., Witzel, U., & Preuschoft, H. (2005). Mechanical stress as the main factor in skull design of the fossil reptile *Proterosuchus* (Archosauria). In: *Bionik*. Springer, Berlin, Heidelberg. https://doi.org/10.1007/3-540-26948-7_31
- Shapiro, M. D., & Jenkins, F. A. (2001). A cynodont from the Upper Triassic of East Greenland: tooth replacement and double-rootedness. *Bulletin of the Museum of Comparative Zoology*, 156(1), 49–58.
- Scheyer, T. M., Desojo, J. B., & Cerda, I. A. (2014). Bone histology of phytosaur, aetosaur, and other archosauriform osteoderms (Eureptilia, Archosauromorpha). *The Anatomical Record*, 297(2), 240–260. <https://doi.org/10.1002/ar.22849>
- Schuch, P. J., Klein, N., & Lambert, M. (2021). What’s my age again? On the ambiguity of histology-based skeletochronology. *Proceedings of the Royal Society B*, 288(1955), 20211166. <https://doi.org/10.1098/rspb.2021.1166>
- Sellwood, B. W., & Valdes, P. J. (2006). Mesozoic climates: General circulation models and the rock record. *Sedimentary geology*, 190(1–4), 269–287. <https://doi.org/10.1016/j.sedgeo.2006.05.013>
- Sereno, P. C. (1991). Basal archosaurs: phylogenetic relationships and functional implications. *Journal of Vertebrate Paleontology*, 11(S4), 1–53. <https://doi.org/10.1080/02724634.1991.10011426>
- Smith, J. B., Vann, D. R., & Dodson, P. (2005). Dental morphology and variation in theropod dinosaurs: implications for the taxonomic identification of isolated teeth. *The Anatomical Record Part A: Discoveries in Molecular, Cellular, and Evolutionary Biology: An Official Publication of the American Association of Anatomists*, 285(2), 699–736. <https://doi.org/10.1002/ar.a.20206>
- Spielmann, J. A., & Lucas, S. G. (2012). Tetrapod Fauna of the Upper Triassic Redona Formation East-central New Mexico: The Characteristic Assemblage of the Apachean Land-vertebrate Faunachron. *New Mexico Museum of Natural History and Science Bulletin*, 55.
- Stocker, M. R. (2010). A new taxon of phytosaur (Archosauria, Pseudosuchia) from the Late Triassic (Norian) Sonsela Member (Chinle Formation) in Arizona, and a critical reevaluation of *Leptosuchus* Case, 1922. *Palaeontology*, 53(5), 997–1022. <https://doi.org/10.1111/j.1475-4983.2010.00983.x>
- Stocker, M. R. (2012). A new phytosaur (Archosauriformes, Phytosauria) from the Lot’s Wifebeds (Sonsela Member) within the Chinle Formation (Upper Triassic) of Petrified Forest National Park, Arizona. *Journal of Vertebrate Paleontology*, 32(3), 573–586. <https://doi.org/10.1080/02724634.2012.649815>
- Stocker, M.R., & Butler, R. J. (2013). Phytosauria. In: Nesbitt SJ, Desojo JB, Irmis RB, eds. *Anatomy, phylogeny and palaeobiology of early archosaurs and their kin*. London: Geological Society, Special Publication, 379, 91–117. <https://doi.org/10.1144/SP379.5>
- Stocker, M. R., Zhao, L. J., Nesbitt, S. J., Wu, X. C., & Li, C. (2017). A short-snouted, Middle Triassic phytosaur and its implications for the morphological evolution and biogeography of Phytosauria. *Scientific Reports*, 7(1), 1–9. <https://doi.org/10.1038/srep46028>
- Sulej, T., Wolniewicz, A., Bonde, N., Błazejowski, B., Niedźwiedzki, G., & Tałanda, M. (2014). New perspectives on the Late Triassic vertebrates of East Greenland: preliminary results of a Polish–Danish palaeontological expedition. *Polish Polar Research*, 35(4), 541–552.
- Sulej, T., Krzesiński, G., Tałanda, M., Wolniewicz, A. S., Błazejowski, B., Bonde, N., Gutowski, P., Sienkiewicz, M., & Niedźwiedzki, G. (2020). The earliest-known mammaliaform fossil from Greenland sheds light on origin of mammals. *Proceedings of the National Academy of Sciences*, 117(43), 26861–26867. <https://doi.org/10.1073/pnas.2012437117>
- Teschner, E. M., Konietzko-Meier, D., & Klein, N. (2022). Growth and limb bone histology of aetosaurs and phytosaurs from the Late Triassic Krasiejów locality (sw Poland) reveals strong environmental influence on growth pattern. *Contributions to Zoology*, 91, 199–232.
- von Meyer, H. (1863). Der Schädel des *Belodon* aus dem Stubensandstein des oberen Keupers. [The skull of *Belodon* from the Stubensandstein of the upper Keuper] *Palaeontographica*, 10, 227–246.
- von Meyer, H., and Plieninger, T. (1844). Beiträge zur Paläontologie Württemberg’s: enthaltend die fossilen wirbelthierreste aus den triasgebilden mit besonderer rücksicht auf die Labyrinthodonten des Keupers. [Contributions to Württemberg’s paleontology: containing the fossil remains of vertebrates from the Triassic formations with special reference to the labyrinthodonts of Keuper] *E. Schweizerbart*, 132, 12.
- Weems, R. E. (1979). A large parasuchian (phytosaur) from the Upper Triassic portion of the Culpeper Basin of Virginia (USA). *Proceedings of the Biological Society of Washington*, 92(4), 682–688.
- Weems, R. E. (2018). A synopsis of the vertebrate fauna from the Culpeper Basin (Upper Triassic–Lower Jurassic, Maryland and Virginia). *New Mexico Museum of Natural History and Science Bulletin*, 79, 749–768.
- Zeigler, K. E., Heckert, A. B., & Lucas, S. G. (2003a). An illustrated atlas of the phytosaur (Archosauria: Parasuchidae) postcrania from the Upper Triassic Snyder Quarry (Petrified Forest Formation, Chinle Group). *Paleontology and Geology of the Upper Triassic (Revue) Snyder Quarry, New Mexico: Bulletin*, 24, 89–103.
- Zeigler, K. E., Heckert, A. B., & Lucas, S. G. (2003b). Phytosaur (Archosauria: Parasuchidae) cranial and mandibular material from the Upper Triassic Snyder Quarry (Petrified Forest Formation, Chinle Group). *Paleontology and Geology of the Upper Triassic (Revue) Snyder Quarry, New Mexico: Bulletin*, 24, 81–88.

Handling Editor: Pia Viglietti.
Phylogenetics Editor: Pedro Godoy.